Office of Naval Research
Contract Nonr-1866 (32) NR-371-016

ON THE ELECTRICALLY THICK CYLINDRICAL ANTENNA

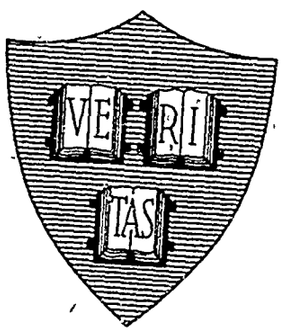

By
David C. Chang

August 1966

Technical Report No. 509

Division of Engineering and Applied Physics
Harvard University • Cambridge, Massachusetts

Office of Naval Research
Contract Nonr-1866(32)
NR - 371 - 016

ON THE ELECTRICALLY THICK CYLINDRICAL ANTENNA

by

David C. Chang

Technical Report No. 509

August, 1966

The research reported in this document was made possible through support extended to Cruft Laboratory, Harvard University, by the U.S. Army Research Office, the U.S. Air Force Office of Scientific Research, and the U.S. Office of Naval Research under the Joint Services Electronics Program by Contract Nonr-1866(32).

Cruft Laboratory

Division of Engineering and Applied Physics

Harvard University

Cambridge, Massachusetts

ON THE ELECTRICALLY THICK CYLINDRICAL ANTENNA

by

David C. Chang

Division of Engineering and Applied Physics

Harvard University, Cambridge, Massachusetts

ABSTRACT

The problem of a thick cylindrical antenna driven by a "delta-function generator" is investigated. Numerical solutions are obtained for two different mathematical models – one is driven by a "delta-function generator" on both outside and inside surfaces of the antenna, and another is driven only on the outside surface. In both cases, current singularity near the driven point has been taken care of and subsequently subtracted out, before the numerical solution is applied. For antennas with circumferences less than a free-space wavelength, the results are compared with the experimental data obtained by Holly [12]. For antennas with larger radii, no experimental data are yet available.

I. INTRODUCTION

In the theory of linear antenna, the total current distribution along an antenna with axial symmetry can usually be obtained by solving an integral equation. It is well known that the integral equation of the dipole antenna can be written as [1]

$$\int_{-h}^{+h} k_o I_t(z')\, K(z-z';a)\, dz' = \frac{i4\pi}{\zeta_o}\left(C\cos k_o z + \frac{1}{2} V \sin k_o|z|\right); \qquad |z| \leq h \tag{1}$$

where

$$K(z-z';a) = \frac{1}{2\pi}\int_{-\pi}^{+\pi} d\theta\, \frac{e^{+ik_o\sqrt{(z-z')^2 + (r^2+a^2-2ra\cos\theta)}}}{\sqrt{(z-z')^2 + (r^2+a^2-2ra\cos\theta)}} \tag{2}$$

k_o the free space wave number and ζ_o the characteristic impedance of free space (i.e., 120 π ohm). The integral equation (1), which is satisfied by the total current distribution $I_t(z)$ on the antenna, corresponds exactly to the mathematical model of a tubular dipole antenna which has a half-length h and radius a (Fig. 1a). Near the origin, z = 0, the antenna is dirven by a so-called "δ-generator" of vcltage V, such that the tangential electric field $E_Z(z)$ on both outer and inner surfaces of the antenna is given by

$$E_Z(z) = -V\delta(z). \tag{3}$$

For antennas with very thin radius, various methods have been developed for solving this integral equation. For example, King-Middleton in 1946 had already obtained a second-order iterated solution [2]. Tai in 1950 used a variational technique to obtain a first-order

solution whose input impedance is stationary [3]. King in 1959, and King-Wu again in 1964 derived a two-term and three-term theory for the current [4]. Wu in 1956 applied the Weiner-Hopf technique to the problem of the long antenna [5]. Duncan-Hinchey in 1960 used the Fourier-series-expansion technique [6] and Mei in 1964 obtained a numerical solution for the current distribution [7]. The solutions obtained by these authors were, in one way or another, based upon an approximation of the kernel $K(z-z';a)$ of the integral equation. These approximations are satisfactory only when the radius of the antenna is very small compared with the free-space wavelength and, therefore, cannot be applied directly to the antenna with moderately large radius.

Moreover, as pointed out recently by King and Wu [8], the model corresponding to Eq. (1) does not agree precisely with what is used in the experiment. Experimentally, the usual coaxial-line-driven antenna over a ground plane is excited only from the outside and not from both sides of the antenna (Fig. 1b). In order to represent the experimental model, an extra term has to be added into Eq. (1), i.e.,

$$\int_{-h}^{+h} k_o I_t(z')\, K(z-z';a)\, dz' = \frac{i4\pi}{\zeta_o}\left(C\cos k_o z + \frac{V}{2}\sin|k_o z|\right) + \frac{i2\pi k_o^2}{\zeta_o} V \int_0^a r'\, dr'\, K(z-z';r')\Big|_{z'=0}; \qquad |z| \leq h. \tag{1a}$$

As is shown later, this extra term in Eq. (1a) is in the order of $(k_o a)^2$ and therefore can be neglected for thin antenna. Eq. (1a) then reduces to Eq. (1). This, however, may not be true for antennas with moderately large radii.

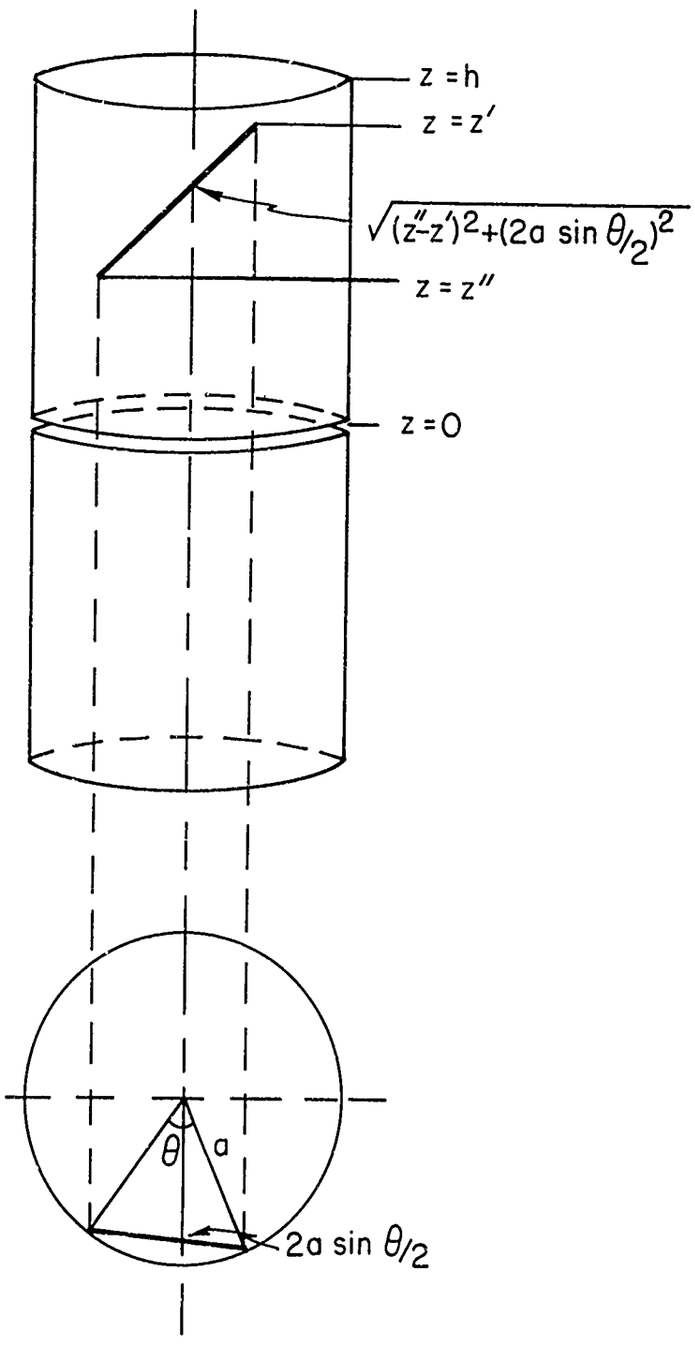

FIG. (1a)

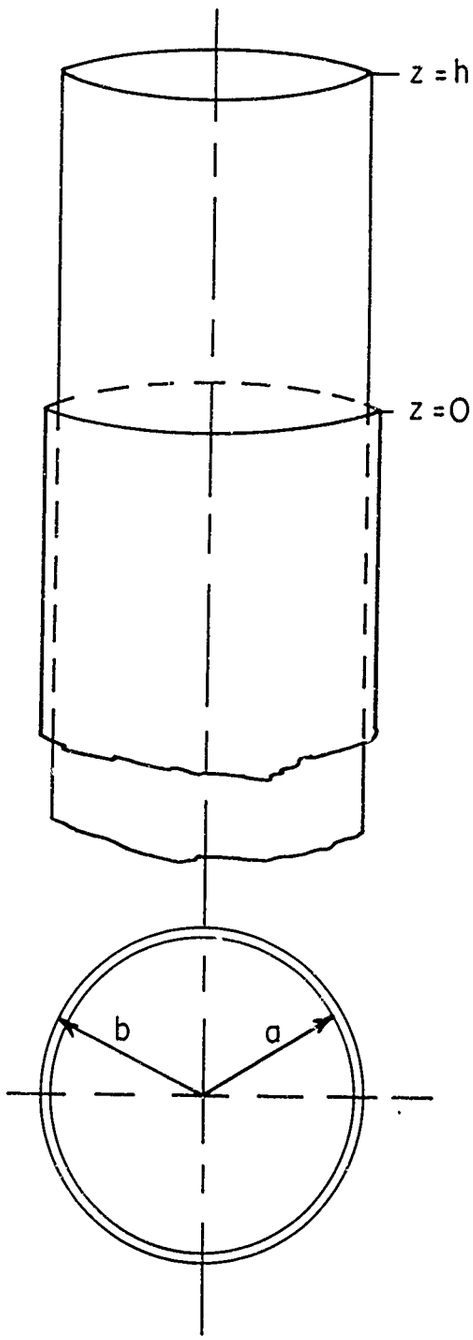

FIG. (1b)

On the other hand, with the help of the modern high-speed computer, integral equations of this type (i. e., Eqs. (1) and (1a)) can actually be solved numerically by a so-called "approximate product-integration technique," even when the exact kernel, which has a singularity at $z = z'$, is retained. The purpose of this report is to apply this method to the thick antenna.

II. DIPOLE ANTENNA WITH 2-SIDED EXCITATION

A. CURRENT BEHAVIOR NEAR THE DRIVING POINT

Let $Z = k_o z$, $H = k_o h$, $A = k_o a$ so that Eq. (1) can be normalized as follows:

$$\int_{-H}^{+H} I_t(Z')\, K(Z-Z';A)\, dZ' = \frac{i4\pi}{\zeta_o}\left(C\cos Z + \frac{1}{2} V \sin|Z|\right); \quad |Z| \leq H. \qquad (4)$$

The boundary condition at both ends of the antenna requires the total current $I_t(Z')$ to vanish, i.e.,

$$I_t(\pm H) = 0.$$

In order to solve Eq. (4) numerically, the integral on the left must be approximated by a sum of products of some weighting functions and the values of $I_t(Z)$ at certain sample points. Hence, any singularity in the current that appears in the solution of Eq. (4) must be evaluated first and subtracted out from the integral in order to assure a good approximation. From the analysis of thin antennas, it is well understood that the singular part of $I_t(Z)$ is due directly to the existence of the non-physical δ-function source, and that this part of the current is independent of the antenna length. That is, when $H \to \infty$, Eq. (1) will degenerate into

$$\int_{-\infty}^{+\infty} I_t(Z')\, K(Z-Z';A)\, dZ' = \frac{2\pi V}{\zeta_o} e^{+i|Z|} = M(Z); \qquad -\infty < Z < \infty \qquad (4a)$$

Now define the Fourier transforms of $I_t(Z)$, $M(Z)$ and $K(Z-Z';A)$ as $I_t(\lambda)$, $M(\lambda)$ and $K(\lambda, A)$, respectively,

$$\begin{cases} I_t(Z) = \int_C I_t(\lambda)\, e^{-i\lambda Z}\, d\lambda & (5a) \\ I_t(\lambda) = \frac{1}{2\pi} \int_{-\infty}^{+\infty} I_t(Z)\, e^{+i\lambda Z}\, dZ & (5b) \end{cases}$$

$$M(Z) = \int_C M(\lambda)\, e^{-i\lambda Z}\, d\lambda \qquad (6a)$$

$$M(\lambda) = \frac{1}{2\pi} \int_{-\infty}^{+\infty} \frac{2\pi V}{\zeta_o}\, e^{+i|Z|}\, e^{+i\lambda Z}\, dZ$$

$$= \frac{i2V}{\zeta_o} \frac{1}{1-\lambda^2} \qquad (6b)$$

and

$$K(Z, R) = \int_C K(\lambda, R)\, e^{-i\lambda Z}\, d\lambda$$

$$K(\lambda, R) = \frac{1}{2\pi} \int_{-\infty}^{+\infty} K(Z, R)\, e^{+i\lambda Z}\, dZ \qquad (7b)$$

Since the kernel $K(Z-Z'; R)$ is the free space Green's function of a ring source which is distributed on the surface of the antenna, the Fourier transform of the Green function can be substituted in Eq. (7b). Thus,

$$K(\lambda, R) = \frac{i}{4\pi} \int_{-\pi}^{+\pi} H_o^{(1)}\left(\sqrt{1-\lambda^2}\sqrt{R^2+A^2-2RA\cos\theta}\right) d\theta$$

$$= \frac{i}{4\pi} \int_{-\pi}^{+\pi} d\theta \sum_{n=-\infty}^{+\infty} H_n^{(1)}\left(R_> \sqrt{1-\lambda^2}\right) J_n\left(R_< \sqrt{1-\lambda^2}\right) e^{+in\theta}$$

$$= \frac{i}{2} H_o^{(1)}\left(R_> \sqrt{1-\lambda^2}\right) J_o\left(R_< \sqrt{1-\lambda^2}\right) \qquad (7c)$$

where $R_{\substack{> \\ <}} = \substack{\max \\ \min}(R, A)$. The branch cuts at $\lambda = \pm 1$ and the path of integration C are shown in Fig. 2. The choice of these branch cuts is, in principle, quite arbitrary. One criterion is that the solution obtained for $|\lambda| < 1$ on the real axis should be in agreement with the solution obtained for $|\lambda| > 1$, also on the axis, after detouring around the branch point. However, for the convenience of numerical integration, the branch cuts actually chosen are the following:

$$\begin{aligned}
&\text{(i)} && \sqrt{\lambda^2 - 1} = \sqrt{\lambda^2 - 1} && |\lambda| > 1 \text{ on the real axis;} \\
&\text{(ii)} && \sqrt{\lambda^2 - 1} = -i\left|\sqrt{\lambda^2 - 1}\right| && \text{on the } \substack{\text{right} \\ \text{left}} \text{ hand side of the } \substack{\text{left} \\ \text{right}} \text{ branch cut;} \\
&\text{(iii)} && \sqrt{\lambda^2 - 1} = +i\left|\sqrt{\lambda^2 - 1}\right| && \text{on the } \substack{\text{left} \\ \text{right}} \text{ hand side of the } \substack{\text{left} \\ \text{right}} \text{ branch cut;} \\
&\text{(iv)} && \left|\arg\sqrt{\lambda^2 - 1}\right| < \frac{\pi}{2} && \text{elsewhere.}
\end{aligned} \tag{8}$$

With the branch cuts defined above, (5), (6) can be substituted in (4a), and use made of the convolution theorem. Then

$$2\pi I_t(\lambda)\, K(\lambda, A) = \frac{iV}{\pi}\left(\frac{2\pi}{\zeta_o}\right)\frac{1}{1 - \lambda^2}$$

$$I_t(\lambda) = \frac{2V}{\pi\zeta_o}\,\frac{1}{(1-\lambda^2)\, H_o^{(1)}\left(A\sqrt{1-\lambda^2}\right)\, J_o\left(A\sqrt{1-\lambda^2}\right)} \tag{9}$$

or

$$I_t(Z) = \frac{2V}{\pi\zeta_o}\int_C d\lambda\, e^{-i\lambda Z}\,\frac{1}{(1-\lambda^2)\, H_o^{(1)}\left(A\sqrt{1-\lambda^2}\right)\, J_o\left(A\sqrt{1-\lambda^2}\right)}$$

$$= \frac{4V}{\pi\zeta_o}\int_0^\infty d\lambda\,\frac{\cos\lambda Z}{(1-\lambda^2)\, H_o^{(1)}\left(A\sqrt{1-\lambda^2}\right)\, J_o\left(A\sqrt{1-\lambda^2}\right)} \tag{10}$$

Here, since the integrand behaves as $\frac{1}{\epsilon \ln \epsilon}$ near the branch point (i. e., $\lambda = 1 + \epsilon e^{+i\theta}$), the integration around the branch point vanishes as $\epsilon \to 0$.

Although the expression for $I_t(Z)$ for all Z is rather difficult to obtain, the leading term in $I_t(Z)$ near $Z = 0$ can be obtained directly from Eq. (10). That is, if λ_o is assumed to be a large number such that $\lambda_o \gg 1$, $A\sqrt{1 + \lambda_o^2} \gg 1$, the integral can be split into two parts, one evaluated from $0 \to \lambda_o$, the other from λ_o to ∞. For the integral from λ_o to ∞, use can be made of the asymptotic expressions for the Bessel function,

$$I_t(Z) = \frac{4V}{\pi\zeta_o}\left\{\int_0^{\lambda_o} d\lambda \frac{\cos \lambda Z}{(1-\lambda^2) H_o^{(1)}\left(A\sqrt{1-\lambda^2}\right) J_o\left(A\sqrt{1-\lambda^2}\right)} + (-i\pi A) \int_{\lambda_o}^{\infty} \frac{\cos \lambda Z}{\lambda} d\lambda\right\}$$

$$= \frac{4V}{\pi\zeta_o}\left\{\int_0^{\lambda_o} d\lambda \frac{\cos \lambda Z}{(1-\lambda^2) H_o^{(1)}\left(A\sqrt{1-\lambda^2}\right) J_o\left(A\sqrt{1-\lambda^2}\right)} + i\pi A\, Ci(\lambda_o Z)\right\}. \tag{11}$$

Here, $Ci(\lambda_o Z)$ is the cosine integral whose behavior near $\lambda_o Z \to 0$ is known as

$$Ci(\lambda_o Z) = \gamma + \ln \lambda_o Z + \sum_{n=1}^{\infty} \frac{(-1)^n (\lambda_o Z)^{2n}}{2n(2n)!}. \tag{12}$$

The substitution of Eq. (12) into Eq. (11) gives

$$I_t(Z) \sim \frac{i4VA}{\zeta_o} \ln \lambda_o Z \qquad \text{as } Z \to 0. \tag{13}$$

This logarithmic term, of course, had been observed early in 1959 by

King and Wu [9]. Also, since this logarithmic term represents a purely local effect due to the δ-function, it should be essentially unchanged for an antenna of finite length.

B. NUMERICAL SOLUTION FOR THE CURRENT DISTRIBUTION – THE "APPROXIMATE PRODUCT-INTEGRATION TECHNIQUE"

1. Total Current Distribution

To solve the integral equation numerically, each half of the antenna is first divided into N equally spaced segments so that each segment has the length 2Δ where $\Delta = \frac{H}{2N}$. Furthermore, if $Z_n = (n-1)\Delta$, $n = 1, 2, \ldots,$ $2N+1$ (Fig. 3), the right-hand side of Eq. (4) can be written as the sum of N integrals. The n^{th} integral in the equation is

$$\int_{-\Delta}^{+\Delta} I_t(Z'+Z_{2n})[K(Z-Z'-Z_{2n})+K(Z+Z'+Z_{2n})]\,dZ'. \tag{14}$$

In this segment, let it be assumed that $I_t(Z)$ can be approximated by

$$I_t(Z) = \sum_{s=1}^{M} a_{sn}(Z-Z_{2n})^{s-1} + \delta_{n1}\left(\frac{i4AV}{\zeta_o}\right)\ln\frac{Z}{2\Delta} \tag{15}$$

where δ_{n1} is equal to 1 if $n = 1$ and 0 if $n \neq 1$. The first part in Eq. (15) actually corresponds to the first M terms in the Taylor series expansion about the center of this segment. Thus, the choice of M and the accuracy of the approximation depends upon the true solution $I_t(Z)$ and its derivatives. The second part in Eq. (15) is a logarithmic term which exists only in the first segment and is normalized to vanish at the end of the segment.

BLANK PAGE

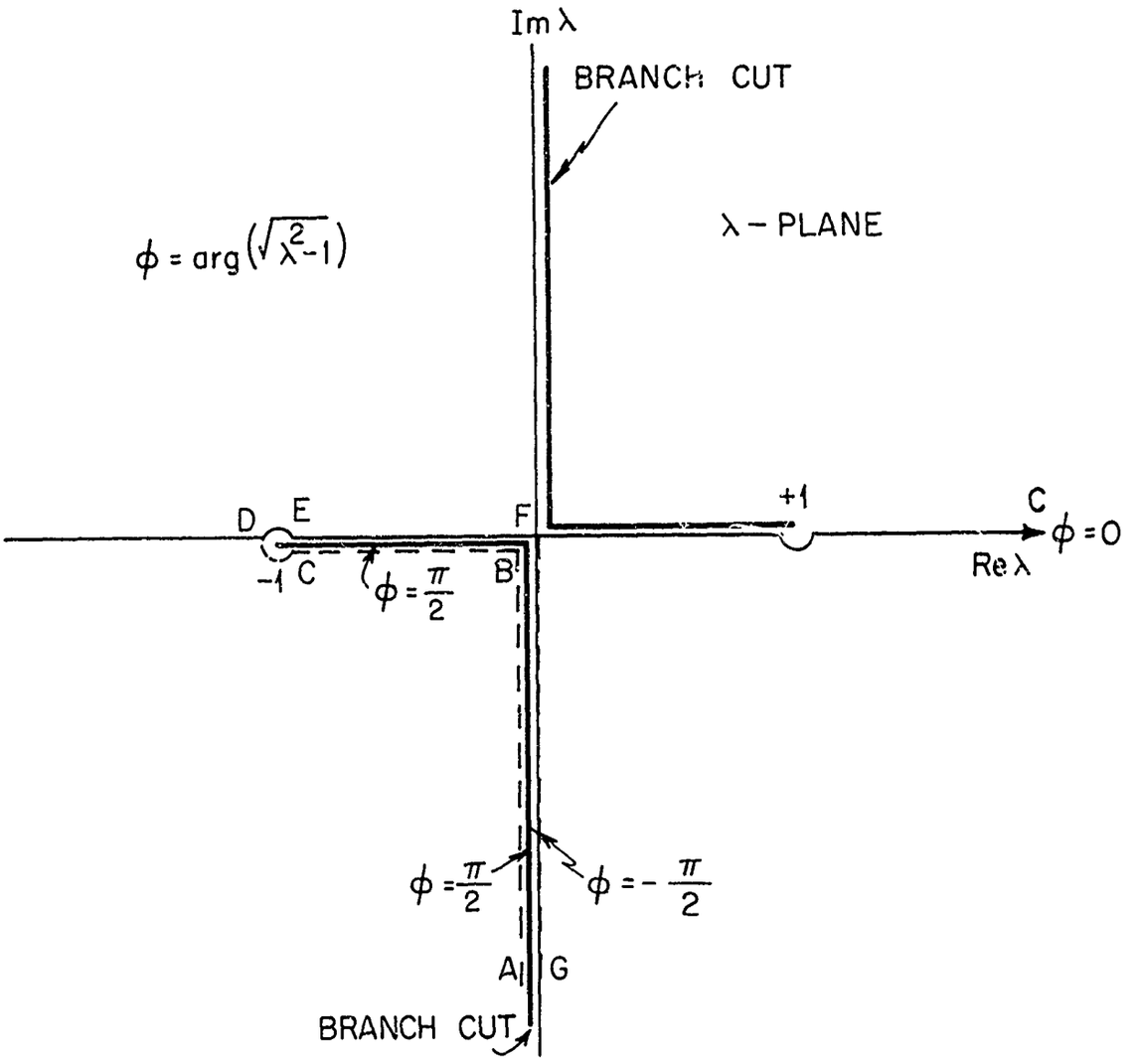

FIGURE 2

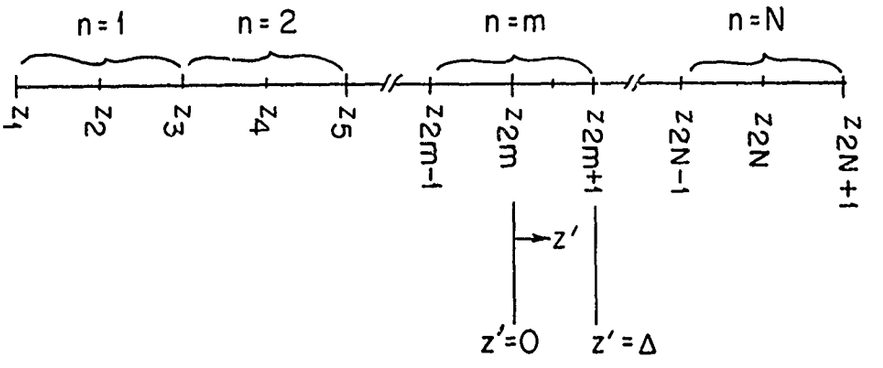

FIGURE 3

Now let u_j with $j = 1, 2, \ldots M$ be the M sample points in the segment and let the integral in (14) be expressed as a sum of the products of some "weighting functions" $a_{nj}^{(t)}(Z)$ and the values of $I_t(Z)$ at the sample points, i.e.,

$$\int_{-\Delta}^{+\Delta} I_t(Z'+Z_{2n})[K(Z-Z'-Z_{2n})+K(Z+Z'+Z_{2n})]\,dZ'$$

$$= \sum_{j=1}^{M} a_{nj}^{(t)}(Z)\, I_t(u_j) + \delta_{n1} f^{(t)}(Z), \tag{16}$$

where

$$f^{t}(Z) = \frac{i4VA}{\zeta_o} \int_{-\Delta}^{+\Delta} \ln \frac{(Z'+\Delta)}{2\Delta} [K(Z-Z'-Z_{2n})+K(Z+Z'+Z_{2n})]\,dZ' \tag{17}$$

and the $a_{nj}^{(t)}(Z)$ are to be determined. Equation (15) is then substituted on both sides of Eq. (16) to give:

$$\sum_{s=1}^{M} a_{sn}\left\{\Delta^{s-1} \int_{-\Delta}^{+\Delta} \left(\frac{Z'}{\Delta}\right)^{s-1} [K(Z-Z'-Z_{2n})+K(Z+Z'+Z_{2n})]\,dZ' \right.$$

$$\left. - \sum_{j=1}^{M} a_{nj}^{(t)}(Z)(u_j-Z_{2n})^{s-1}\right\} = 0$$

or

$$\sum_{s=1}^{M} a_{sn}\left[\Delta^{s-1}\mu_{ns}^{(t)}(Z) - \sum_{j=1}^{M} a_{nj}^{(t)}(Z)(u_j-Z_{2n})^{s-1}\right] = 0; \tag{18}$$

$\mu_{ns}^{(t)}(Z)$ is called the "moment function." Since Eq. (18) is true for any a_{sn}, each term in the summation is zero. Therefore

$$\begin{bmatrix} 1 & 1 & \cdots & 1 \\ \left(\frac{u_1 - Z_{2n}}{\Delta}\right) & \left(\frac{u_2 - Z_{2n}}{\Delta}\right) & & \left(\frac{u_M - Z_{2n}}{\Delta}\right) \\ \left(\frac{u_1 - Z_{2n}}{\Delta}\right)^2 & & & \\ \vdots & & \vdots & \\ \left(\frac{u_1 - Z_{2n}}{\Delta}\right)^{M-1} & & & \left(\frac{u_M - Z_{2n}}{\Delta}\right)^{M-1} \end{bmatrix} \begin{bmatrix} a_{n1}^{(t)}(Z) \\ a_{n2}^{(t)}(Z) \\ \\ \vdots \\ a_{n,M}^{(t)}(Z) \end{bmatrix} = \begin{bmatrix} \mu_{n,1}^{(t)}(Z) \\ \mu_{n,2}^{(t)}(Z) \\ \\ \vdots \\ \mu_{n,M}^{(t)}(Z) \end{bmatrix} \tag{19}$$

or simply,

$$\mathcal{X}_n \alpha_n^{(t)} = \mu_n^{(t)} \tag{19a}$$

where $\alpha_n^{(t)} = \{a_{n,j}^t(Z)\}_j$, $\mu_n^{(t)} = \{\mu_{n,j}^{(t)}(Z)\}_j$, and $\mathcal{X}_n = \left\{\left(\frac{u_j - Z_{2n}}{\Delta}\right)^{i-1}\right\}_{j,i}$. Multiplication of both sides of (19a) by the inverse matrix of $\mathcal{X}_n$ yields the expression for $a_{n,j}^{(t)}$ in terms of the moment function $\mu_{n,j}^{(t)}(Z)$.

The error involved in Eq. (19) is essentially due to the remaining terms in the Taylor series expansion. It is possible to estimate this error and to "throw it back" to improve the solution, but this will not be discussed here [10]. Also, Eq. (19) can be simplified further if $I_t(Z)$ is assumed to be approximated by a lower-order polynomial and M to be a set of equally spaced sample points. For a parabolic approximation, let $M = 3$ and $u_j = Z_{2n-1} + (j-1)\Delta = Z_{2n+j-2}$. Then

$$\mathcal{X}_n = \begin{bmatrix} 1 & 1 & 1 \\ -1 & 0 & 1 \\ 1 & 0 & 1 \end{bmatrix} \tag{20a}$$

The substitution of (20a) into (19a) leads to an explicit expression for $a_{nj}(Z)$.

$$\begin{cases} a^{(t)}_{n,1}(Z) = \frac{1}{2}\left[-\mu^{(t)}_{n,2}(Z) + \mu^{(t)}_{n,3}(Z)\right] \\ a^{(t)}_{n,2}(Z) = \mu^{(t)}_{n,1}(Z) - \mu^{(t)}_{n,3}(Z) \\ a^{(t)}_{n,3}(Z) = \frac{1}{2}\left[\mu^{(t)}_{n,2}(Z) + \mu^{(t)}_{n,3}(Z)\right] \end{cases} \tag{20b}$$

With Eqs. (16) and (20b), Eq. (4a) becomes

$$\sum_{n=1}^{N}\sum_{j=1}^{3} a^{(t)}_{nj}(Z)\, I_t(Z_{2n-2+j}) + f^{(t)}(Z) = \frac{i4\pi}{\zeta_o}\left(C\cos Z + \frac{V}{2}\sin|Z|\right); \qquad Z \leqslant H, \tag{21}$$

or simply, at $Z = Z_K$,

$$\sum_{m=1}^{2N+1} \beta_{Km} I^{(t)}_m + f^{(t)}_K = \frac{i4\pi}{\zeta_o}\left(C\cos Z_K + \frac{V}{2}\sin Z_K\right); \qquad K = 1, 2, \ldots 2N+1, \tag{22}$$

where

$$\begin{cases} \beta^{(t)}_{K1} = a^{(t)}_{1,1}(Z_K) \\ \beta^{(t)}_{K,2S} = a^{(t)}_{S,2}(Z_K); & S = 1, 2, \ldots N \\ \beta^{(t)}_{K,2S-1} = a^{(t)}_{S,1}(Z_K) + a^{(t)}_{S-1,3}(Z_K); & S = 1, 2, \ldots N \\ \beta^{(t)}_{K,2N+1} = a^{(t)}_{N,3}(Z_K). \end{cases} \tag{23}$$

Since the current $I_t(Z)$ must vanish at the ends, I_{2N+1} can be set equal to zero. Equation (22) then involves only 2N+1 unknowns. Thus, if $I_{2N+1} = C$

and $\beta_{K,\,2N+1} = \frac{-i4\pi}{\zeta_o} \cos Z_K$ are redefined, Eq. (22) can be rewritten as follows:

$$\sum_{m=1}^{2N+1} \beta_{Km}^{(t)} I_m^{(t)} = \frac{i2\pi}{\zeta_o} V \sin Z_K - f_K; \qquad K = 1, 2, \ldots 2N+1 \qquad (24a)$$

or simply,

$$\mathcal{\beta}_t \cdot \mathcal{I}_t = \mathcal{Q} \qquad (24b)$$

where $\mathcal{\beta}_t = \{\beta_{Km}^{(t)}\}_{K,\,m}$, $\mathcal{I}_t = \{I_m^{(t)}\}_m$, and $\mathcal{Q} = \left\{\frac{i2\pi}{\zeta_o} V \sin Z_K - f_K\right\}_K$. The multiplication by the inverse matrix of $\mathcal{\beta}_t$ on both sides of (24b) allows the values of $I_t(Z)$ at the sample points to be obtained.

2. Outside and Inside Current Distributions

For any point (Z, R) in air, the magnetic field due to the current distribution on the antenna can be expressed as the curl of the vector potential,

$$B_\theta(Z, R) = (\nabla \times \vec{A})_\theta = \frac{-K_o}{4\pi\nu_o} \frac{\partial}{\partial R} \int_{-H}^{+H} I_t(Z')\, K(Z-Z'; R)\, dZ'. \qquad (25)$$

Thus, the parts of the current, which are distributed, respectively, on the outer and inner surface of the antenna, can be determined from the boundary condition on this surface,

$$I_{\substack{out \\ in}}(Z) = \pm 2\pi\nu_o a B_\theta(Z, R=A\pm\epsilon)$$

$$= \mp \frac{A}{2} \left[\frac{\partial}{\partial R} \int_{-H}^{+H} I_t(Z')\, K(Z-Z'; R)\, dZ'\right]_{R=A\pm\epsilon}; \quad \text{as } \epsilon \to 0. \qquad (26)$$

The difference between these two currents is

$$I_d(Z) = I_{out}(Z) - I_{in}(Z) \tag{27a}$$

$$= -\frac{A}{2}\left[\frac{\partial}{\partial R}\int_{-H}^{+H} I_t(Z')\,K(Z-Z';R)\,dZ'\right]_{R=A+\epsilon}$$

$$+\frac{A}{2}\left[\frac{\partial}{\partial R}\int_{-H}^{+H} I_t(Z')\,K(Z-Z';R)\,dZ'\right]_{R=A-\epsilon} \quad ; \quad \text{as } \epsilon \to 0$$

$$= -\frac{A}{2}\int_{-H}^{+H} I_t(Z')\left[\frac{\partial}{\partial R}K(Z-Z';R)\Big|_{R=A+\epsilon} + \frac{\partial}{\partial R}K(Z-Z';R)\Big|_{R=A-\epsilon}\right] dZ';$$

$$\text{as } \epsilon \to 0.$$

(27)

The interchange of differentiation and integration in the last step of Eq. (27) is not necessarily true for I_{out} or I_{in} alone.

A comparison of (27) with the left-hand side of Eq. (4a) leads to the definitions

$$\mu_{ns}^{(d)}(Z) = \int_{-\Delta}^{+\Delta}\left(\frac{Z'}{\Delta}\right)^{s-1}\left\{-\frac{A}{2}\left[\frac{\partial}{\partial R}K(Z-Z'-Z_{2n};R)\Big|_{R=A+\epsilon} + \frac{\partial}{\partial R}K(Z-Z'-Z_{2n};R)\Big|_{R=A-\epsilon}\right]\right.$$

$$\left.-\frac{A}{2}\left[\frac{\partial}{\partial R}K(Z+Z'+Z_{2n};R)\Big|_{R=A+\epsilon} + \frac{\partial}{\partial R}K(Z+Z'+Z_{2n};R)\Big|_{R=A-\epsilon}\right]\right\} dZ'$$

$$\text{as } \epsilon \to 0$$

(28)

and

$$f^{(d)}(Z) = \frac{i4VA}{\zeta_o} \int_{-\Delta}^{+\Delta} \ln \frac{(Z'+\Delta)}{2\Delta} \left\{ -\frac{A}{2} \left[\frac{\partial}{\partial R} K(Z-Z'-Z_{2n};R) \Big|_{R=A+\epsilon} + \frac{\partial}{\partial R} K(Z-Z'-Z_{2n};R) \Big|_{R=A-\epsilon} \right] - \frac{A}{2} \left[\frac{\partial}{\partial R} K(Z+Z'+Z_{2n};R) \Big|_{R=A+\epsilon} + \frac{\partial}{\partial R} K(Z+Z'+Z_{2n};R) \Big|_{R=A-\epsilon} \right] \right\} dZ';$$

$$\text{as } \epsilon \to 0. \qquad (29)$$

Equation (27) can then be transformed into

$$I_d(Z_K) = \sum_{m=1}^{2N} \beta_{Km}^{(d)} I_m^{(t)} + f_K^{(d)}, \qquad (30)$$

where $f_K^{(d)} = f^{(d)}(Z_K)$ and $\beta_{Km}^{(d)}$ are related to the moment functions $\mu_{ns}^{(d)}(Z)$ in the same manner as in Eqs. (20b) and (23). Let Eq. (30) be combined with Eq. (27a) to obtain

$$I_{\substack{out \\ in}}(Z_K) = \frac{1}{2} \left[I_K^{(t)} \pm \left(\sum_{m=1}^{2N} \beta_{Km}^{(d)} I_m^{(t)} + f_K^{(d)} \right) \right] . \qquad (31)$$

C. EVALUATION OF THE MOMENT FUNCTIONS

Define

$$\mu^{(t)}(S,m) = \int_{-\Delta}^{+\Delta} \left(\frac{Z'}{\Delta} \right)^{s-1} K(m\Delta - Z'; A)\, dZ' \qquad (32)$$

$$\mu^{(d)}(s,m) = \int_{-\Delta}^{+\Delta} \left(\frac{Z'}{\Delta}\right)^{s-1} \left(\frac{-A}{2}\right) \left\{ \frac{\partial}{\partial R} K(m\Delta - Z'; R)\Big|_{R=A+\epsilon} - \frac{\partial}{\partial R} K(m\Delta - Z'; R)\Big|_{R=A-\epsilon} \right\} dZ'; \quad \text{as } \epsilon \to 0. \tag{33}$$

As a consequence of the symmetry of the kernel, i. e., $K(Z,R) = K(-Z,R)$, the moment functions $\mu^{(t)}(s,m)$ and $\mu^{(d)}(s,m)$ have the following properties:

$$\begin{aligned} &\text{(i)} \quad \mu(s,-m) = (-1)^{s-1}\,\mu(s,m) \\ &\text{(ii)} \quad \mu(1,0) = 2\mu(1,1)\Big|_{\text{as } \Delta \to \frac{\Delta}{2}} \\ &\text{(iii)} \quad \mu(2,0) = 0 \\ &\text{(iv)} \quad \mu(3,0) = \tfrac{1}{2}[\mu(3,1) - 2\mu(2,1) + \mu(1,1)]_{\text{as } \Delta \to \frac{\Delta}{2}} \end{aligned} \tag{34}$$

Equation (34) holds true for both subscripts (t) and (d). A comparison of (34) with the definition for $\mu_{n,s}^{(t),(d)}(Z)$ leads to

$$\mu_{n,s}^{(t),(d)}(Z_K) = \mu^{(t),(d)}(s, K-2n) + \mu^{(t),(d)}(s, -K+2-2n). \tag{35}$$

After the substitution of (35) in Eqs. (20b) and (23), it is possible to express $\beta_{K,m}^{(t),(d)}$ in terms of $\mu^{(t),(d)}(s,m)$ explicitly, i. e.,

$$\begin{aligned} \beta_{K,1} &= \tfrac{1}{2}[\mu(3,|2-K|) + H(2-K)\mu(2,|2-K|) + \mu(3,K) + \mu(2,K)] \\ \beta_{K,2S-1} &= \tfrac{1}{2}[H(2S-K)\mu(2,|2S-K|) + \mu(3,|2S-K|) + \mu(2,2S+K-2) + \mu(3,2S+K-2) \\ &\quad - H(2S-K-2)\mu(2,|2S-K-2|) + \mu(3,|2S-K-2|) - \mu(2,2S+K-4) + \mu(3,2S+K-4)] \\ \beta_{K,2S} &= \mu(1,|2S-K|) - \mu(3,|2S-K|) + \mu(1,2S+K-2) - \mu(3,2S+K-2) \end{aligned} \tag{36}$$

where H(Z) is defined as -1 if $Z < 0$ and 1 if $Z > 0$.

1. Evaluation of $\mu^{(t)}(s,m)$

The substitution of Eq. (7a) and Eq. (7c) in (32) and the interchange of the two integrations gives

$$\mu^{(t)}(s,m) = \frac{i}{2}\int_C d\lambda\, H_o^{(1)}\left(A\sqrt{1-\lambda^2}\right) J_o\left(A\sqrt{1-\lambda^2}\right) \int_{-\Delta}^{+\Delta} dZ' \left(\frac{Z'}{\Delta}\right)^{s-1} e^{+i\lambda(Z'-m\Delta)}$$

$$= \frac{i}{2}\int_C \frac{1}{\lambda} G_S(m,\lambda)\, H_o^{(1)}\left(A\sqrt{1-\lambda^2}\right) J_o\left(A\sqrt{1-\lambda^2}\right) d\lambda, \qquad (37)$$

where

$$G_S(m,\lambda) = -i(1-e^{-i2\lambda\Delta})\, e^{-i(m-1)\lambda\Delta}; \quad S=1$$

$$= -\frac{1}{\lambda\Delta}[(i\lambda\Delta-1)+(i\lambda\Delta+1)\, e^{-i2\lambda\Delta}]\, e^{-i(m-1)\lambda\Delta}; \quad S=2$$

$$= -\left(\frac{1}{\lambda\Delta}\right)^2[(\lambda^2\Delta^2+i2\lambda\Delta-2)-(\lambda^2\Delta^2-i2\lambda\Delta-2)\, e^{-i2\lambda\Delta}]\, e^{-i(m-1)\lambda\Delta}; \quad S=3. \qquad (38)$$

Here, it can easily be seen that $G_S(m,\lambda) \to -i$ as $\lambda \to \infty$, and that $G_S(m,-i\lambda)$ is purely imaginary.

In Eq. (37), aside from the logarithmic singularities at the branch points, the integrand has no other singularity. Furthermore, as $|\lambda| \to \infty$ in the lower half plane,

$$\frac{1}{\lambda} G_S(\lambda)\, H_o^{(1)}\left(A\sqrt{1-\lambda^2}\right) J_o\left(A\sqrt{1-\lambda^2}\right) \sim \text{const}\,\frac{1}{\lambda^2}\, e^{-(m-1)\Delta|Im\lambda|}.$$

Therefore, the contour can be deformed from C to C' for $m \geq 1$,

$$\mu^{(t)}(S,m) = \frac{i}{2}\left(\int_A^B + \int_B^C + \int_E^F + \int_F^H\right)\frac{1}{\lambda} G_S(m,\lambda)\, H_o^{(1)}\left(A\, e^{+\frac{i\pi}{2}\sqrt{\lambda^2-1}}\right)$$

$$\cdot\, J_o\left(A\, e^{+\frac{i\pi}{2}\sqrt{\lambda^2-1}}\right) d\lambda$$

$$= \frac{i}{2}\left(\int_{-i\infty}^{0} + \int_0^{-1}\right)\frac{G_S(m,\lambda)}{\lambda} H_o^{(1)}\left(A\, e^{+i\pi\left|\sqrt{\lambda^2-1}\right|}\right)$$

$$\cdot\, J_o\left(A\, e^{+i\pi\left|\sqrt{\lambda^2-1}\right|}\right) d\lambda$$

$$+ \frac{i}{2}\left(\int_{-1}^{0} + \int_0^{-i\infty}\right)\frac{G_S(m,\lambda)}{\lambda} H_o^{(1)}\left(A\left|\sqrt{\lambda^2-1}\right|\right) J_o\left(A\left|\sqrt{\lambda^2-1}\right|\right) d\lambda$$

$$= \frac{i}{2}\left(\int_0^{-i\infty} + \int_{-1}^{0}\right)\frac{G_S(m,\lambda)}{\lambda} J_o\left(A\left|\sqrt{\lambda^2-1}\right|\right) \cdot$$

$$\left[H_o^{(1)}\left(A\left|\sqrt{\lambda^2-1}\right|\right) + H_o^{(2)}\left(A\left|\sqrt{\lambda^2-1}\right|\right)\right] d\lambda$$

$$= i\int_0^1 \frac{G_S(m,-\lambda)}{-\lambda} J_o^2\left(A\sqrt{1-\lambda^2}\right) d\lambda + \int_0^\infty \frac{G_S(m,-i\lambda)}{-i\lambda} J_o^2\left(A\sqrt{1+\lambda^2}\right) d\lambda. \tag{39}$$

Equation (39) is the final expression for computation. The first integral consists of both real and imaginary parts, and is integrated within a finite interval. The second integral has only a real part and is integrated from $0 \to \infty$; the integrand decays at least as $\frac{1}{\lambda^2}$ as $\lambda \to \infty$. In both integrals, due to the choice of the branch cut, the arguments of the Bessel functions are all real.

Likewise, an expression for $f_K^{(t)}$ can also be obtained (see Appendix).

2. Evaluation of $\mu^{(d)}(m,S)$

The substitution of Eqs. (7a) and (7b) into Eq. (33) gives

$$\mu^{(d)}(s,m) = \frac{i}{2}\int_C d\lambda \left(\frac{A}{2}\right)\sqrt{1-\lambda^2}\left[H_1^{(1)}\left(A\sqrt{1-\lambda^2}\right)J_o\left(A\sqrt{1-\lambda^2}\right)\right.$$
$$\left. + H_o^{(1)}\left(A\sqrt{1-\lambda^2}\right)J_1\left(A\sqrt{1-\lambda^2}\right)\right]\int_{-\Delta}^{+\Delta} dZ' \left(\frac{Z'}{\Delta}\right)^{s-1} e^{-i\lambda Z'}$$
$$= \frac{iA}{4}\int_C \frac{G_S(m,\lambda)}{\lambda}\sqrt{1-\lambda^2}\left[H_1^{(1)}\left(A\sqrt{1-\lambda^2}\right)J_o\left(A\sqrt{1-\lambda^2}\right)\right.$$
$$\left. + H_o^{(1)}\left(A\sqrt{1-\lambda^2}\right)J_1\left(A\sqrt{1-\lambda^2}\right)\right] d\lambda. \qquad (40)$$

As in Eq. (37), the integrand in Eq. (40) also has two branch points at $\lambda = \pm 1$. However, the integrand is finite at these points. On the real axis, as $|\lambda| \to \infty$

$$\frac{G_S(m,\lambda)}{\lambda}\sqrt{1-\lambda^2}\left[H_1^{(1)}\left(A\sqrt{1-\lambda^2}\right)J_o\left(A\sqrt{1-\lambda^2}\right)\right.$$
$$\left. + H_o^{(1)}\left(A\sqrt{1-\lambda^2}\right)J_1\left(A\sqrt{1-\lambda^2}\right)\right]$$
$$\sim \frac{-i}{\pi\lambda} e^{-i(m-1)\lambda\Delta}\left[e^{+i\left(i\lambda A - \frac{3}{4}\pi\right)} e^{-i\left(iA\lambda - \frac{\pi}{4}\right)} + e^{+i\left(i\lambda A - \frac{\pi}{4}\right)} e^{-i\left(i\lambda A - \frac{\pi}{4}\right)}\right]$$
$$+ O\left(\frac{1}{\lambda^2}\right)$$
$$\sim \text{const}\ \frac{1}{\lambda^2}. \qquad (41)$$

Therefore, due to the cancellation of the leading term, Eq. (40) is integrable on the real axis for all $m \geq 1$. However, this is not true on the imaginary axis, since as $|\lambda| \to \infty$,

$$\frac{G_S(m,\lambda)}{\lambda}\sqrt{1-\lambda^2}\left[H_1^{(1)}\left(A\sqrt{1-\lambda^2}\right)J_o\left(A\sqrt{1-\lambda^2}\right)\right.$$
$$\left.+ H_o^{(1)}\left(A\sqrt{1-\lambda^2}\right)J_1\left(A\sqrt{1-\lambda^2}\right)\right]$$
$$\sim \pm\frac{e^{-(m-1)\lambda\Delta}}{\pi\lambda}\left\{e^{i\left(\pm A\lambda-\frac{3}{4}\pi\right)}\left[e^{+i\left(\pm A\lambda-\frac{\pi}{4}\right)}+e^{-i\left(\pm A\lambda-\frac{\pi}{4}\right)}\right]\right.$$
$$\left.+ e^{i\left(\pm A\lambda-\frac{\pi}{4}\right)}\left[e^{i\left(\pm A\lambda-\frac{3\pi}{4}\right)}+e^{-i\left(\pm A\lambda-\frac{3\pi}{4}\right)}\right]\right\}+O\left(\frac{1}{\lambda^2}\right)$$
$$\sim \frac{1}{\lambda}; \tag{42}$$

The (+) and (-) signs correspond to the left- and right-hand sides of the branch cut, respectively. Because the integrand decays as $\frac{1}{\lambda}$ on the imaginary axis, it is not possible to deform the contour. Thus, Eq. (34) can be integrated only along the real axis, as follows:

$$\mu^{(d)}(s,m) = \frac{iA}{4}\int_0^1 \frac{G_S(m,\lambda)-G_S(m,\lambda)}{\lambda}\sqrt{1-\lambda^2}\left[H_1^{(1)}\left(A\sqrt{1-\lambda^2}\right)J_o\left(A\sqrt{1-\lambda^2}\right)\right.$$
$$\left.+ H_o^{(1)}\left(A\sqrt{1-\lambda^2}\right)J_1\left(A\sqrt{1-\lambda^2}\right)\right]d\lambda$$
$$+\frac{A}{\pi}\int_1^\infty \frac{G_S(m,i\lambda)-G_S(m,-i\lambda)}{\lambda}\sqrt{\lambda^2-1}\left[K_1\left(A\sqrt{\lambda^2-1}\right)I_o\left(A\sqrt{\lambda^2-1}\right)\right.$$
$$\left.+ K_o\left(A\sqrt{\lambda^2-1}\right)I_1\left(A\sqrt{\lambda^2-1}\right)\right]d\lambda \tag{43}$$

As in Eq. (39), the first integral consists of both real and imaginary parts, and is integrated within a finite interval. The second integral has only a real part and decays at least as $\frac{1}{\lambda^2}$ as $\lambda \to \infty$. A comparison of (43) with Eq. (39) shows that the second integral in Eq. (43) converges much more slowly than that in Eq. (39).

An expression for $f_K^{(d)}$ can also be obtained (see Appendix).

BLANK PAGE

III. DIPOLE ANTENNA WITH ONE-SIDE EXCITATION

As shown by King and Wu [8], the vector potential $A_Z(Z,R)$, in this case, can be written as follows:

$$A_Z(Z,R) = \frac{1}{4\pi\nu_o}\int_{-H}^{+H} I_t(Z')\,K(Z-Z';R)\,dZ' - \frac{i}{2\nu_o\zeta_o}\,V\,D_o(Z;R), \tag{44}$$

where

$$D_o(Z;R) = \frac{1}{2\pi}\int_0^A R'\,dR' \int_{-\pi}^{+\pi} d\theta\,\frac{e^{\mp i\sqrt{Z^2+(R^2+R'^2-2RR'\cos\theta)}}}{\sqrt{Z^2+(R'^2+R^2-2RR'\cos\theta)}}. \tag{45}$$

The corresponding integral equation for the total current distribution is

$$\int_{-H}^{+H} I_t(Z')\,K(Z-Z';A)\,dZ' = \frac{i4\pi}{\zeta_o}\left(C\cos Z + \frac{V}{2}\sin|Z|\right) + \frac{i2\pi}{\zeta_o}\,V\,D_o(Z;A); \quad |Z| \le H, \tag{46}$$

which is equivalent to Eq. (1a). Since now the δ-function generator exists only on the outside surface of the antenna, the singular current (which is later subtracted out in the numerical solution) should be different from that in the previous case. Aside from this, Eq. (44) is essentially the same as Eq. (4) except that it is necessary to evaluate an extra term which appears in the column matrix $\mathcal{Q}$ in Eq. (24a).

A. CURRENT BEHAVIOR NEAR THE DRIVEN POINT

For an infinitely long antenna, i.e., $H \to \infty$, Eq. (46) degenerates into

$$\int_{-\infty}^{+\infty} I_t(Z')\,K(Z-Z';A)\,dZ' = \frac{2\pi}{\zeta_o}\,V\,e^{+i|Z|} + \frac{i2\pi}{\zeta_o}\,V\,D_o(Z;A); \quad -\infty < Z < \infty. \tag{47}$$

Now, define the Fourier transform of $D_o(Z;R)$ as

$$D_o(Z;R) = \int_C D_o(\lambda;R)\, e^{-i\lambda Z}\, d\lambda \tag{48a}$$

$$D_o(\lambda;R) = \frac{1}{2\pi}\int_{-\infty}^{+\infty} D_o(Z;R)\, e^{+i\lambda Z} dZ$$

$$= \int_0^A R'\, dR' \left(\frac{i}{2}\right) H_o^{(1)}\left(R\sqrt{1-\lambda^2}\right) J_o\left(R'\sqrt{1-\lambda^2}\right)$$

$$= \frac{iA}{2\sqrt{1-\lambda^2}} J_1\left(A\sqrt{1-\lambda^2}\right) H_o^{(1)}\left(R\sqrt{1-\lambda^2}\right) \tag{48b}$$

In the last step in the derivation of Eq. (48b), use has been made of the relationship,

$$\int_0^Z t\, J_o(t)\, dt = Z\, J_1(Z).$$

The substitution of Eqs. (5a-b), (6a-b), (7a-c) and (48a-b) in (47) gives

$$2\pi I_t(\lambda)\left(\frac{i}{2}\right) H_o^{(1)}\left(A\sqrt{1-\lambda^2}\right) J_o\left(A\sqrt{1-\lambda^2}\right)$$

$$= \frac{i2}{\zeta_o} V \frac{1}{1-\lambda^2} - \frac{\pi A}{\zeta_o} V \frac{1}{\sqrt{1-\lambda^2}} J_1\left(A\sqrt{1-\lambda^2}\right) H_o^{(1)}\left(A\sqrt{1-\lambda^2}\right)$$

$$\therefore \quad I_t(\lambda) = \frac{2}{\pi\zeta_o} V \frac{1}{1-\lambda^2} \frac{1}{H_o^{(1)}\left(A\sqrt{1-\lambda^2}\right) J_o\left(A\sqrt{1-\lambda^2}\right)}$$

$$+ \frac{iAV}{\zeta_o} \frac{1}{\sqrt{1-\lambda^2}} \frac{J_1\left(A\sqrt{1-\lambda^2}\right)}{J_o\left(A\sqrt{1-\lambda^2}\right)} \tag{49}$$

Now apply the Wronskian,

$$H_1^{(1)}(Z)\, J_o(Z) - H_o^{(1)}(Z)\, J_1(Z) = \frac{-i2}{\pi}\,\frac{1}{Z}$$

or

$$\frac{1}{H_o^{(1)}(Z)\, J_o(Z)} = \frac{i\pi}{2}\, Z \left(\frac{H_1^{(1)}(Z)}{H_o^{(1)}(Z)} - \frac{J_1(Z)}{J_o(Z)} \right)$$

and the inverse Fourier transform to Eq. (49),

$$I_t(Z) = \frac{iA}{\zeta_o} V \int_C \frac{1}{\sqrt{1-\lambda^2}}\, \frac{H_1^{(1)}\left(A\sqrt{1-\lambda^2}\right)}{H_o^{(1)}\left(A\sqrt{1-\lambda^2}\right)}\, e^{-i\lambda Z}\, d\lambda \qquad (50)$$

For $Z > 0$, and as $\lambda \to \infty$ in the lower half plane,

$$\frac{1}{\sqrt{1-\lambda^2}}\, \frac{H_1^{(1)}\left(A\sqrt{1-\lambda^2}\right)}{H_o^{(1)}\left(A\sqrt{1-\lambda^2}\right)}\, e^{-i\lambda Z} \sim \text{const}\,\frac{1}{\lambda} \cdot e^{-|I_m \lambda|\, Z}.$$

Therefore, the contour can be deformed onto both sides of the branch cut,

$$I_t(Z) = \frac{iA}{\zeta_o} V \left(\int_{-i\infty}^{0} + \int_{0}^{-1} \right) \frac{e^{-i\lambda Z}}{|\sqrt{\lambda^2-1}|\, e^{+i\pi}}\, \frac{H_1^{(1)}\left(A\, e^{+i\pi}|\sqrt{\lambda^2-1}|\right)}{H_o^{(1)}\left(A\, e^{+i\pi}|\sqrt{\lambda^2-1}|\right)}\, d\lambda$$

$$+ \frac{iA}{\zeta_o} V \left(\int_{-1}^{0} + \int_{0}^{-i\infty} \right) \frac{e^{-i\lambda Z}}{|\sqrt{\lambda^2-1}|}\, \frac{H_1^{(1)}\left(A|\sqrt{\lambda^2-1}|\right)}{H_o^{(1)}\left(A|\sqrt{\lambda^2-1}|\right)}\, d\lambda$$

$$= \frac{iA}{\zeta_o} V \left(\int_{-1}^{0} + \int_{0}^{-i\infty} \right) \frac{e^{-i\lambda Z}}{|\sqrt{\lambda^2-1}|} \left[\frac{H_1^{(1)}\left(A|\sqrt{\lambda^2-1}|\right)}{H_o^{(1)}\left(A|\sqrt{\lambda^2-1}|\right)} - \frac{H_1^{(2)}\left(A|\sqrt{\lambda^2-1}|\right)}{H_o^{(2)}\left(A|\sqrt{\lambda^2-1}|\right)} \right] d\lambda$$

(51)

Now apply the Wronskian $H_1^{(1)}(Z)\,H_o^{(2)}(Z) - H_o^{(1)}(Z)\,H_1^{(2)}(Z) = \frac{-i4}{\pi Z}$ to Eq. (51). The result is

$$I_t(Z) = \frac{iA}{\zeta_o} V \left(\int_{-1}^{0} + \int_{0}^{-i\infty} \right) \frac{e^{-i\lambda Z}}{|\sqrt{\lambda^2-1}|} \frac{\frac{-i4}{\pi} \frac{1}{A|\sqrt{\lambda^2-1}|}}{J_o^2\left(A|\sqrt{\lambda^2-1}|\right) + Y_o^2\left(A|\sqrt{\lambda^2-1}|\right)}$$

$$= \frac{4V}{\pi\zeta_o} \left(\int_0^1 \frac{e^{+i\lambda Z}}{J_o^2\left(A\sqrt{1-\lambda^2}\right) + Y_o^2\left(A\sqrt{1-\lambda^2}\right)}\, d\lambda \right.$$

$$\left. - i \int_0^\infty \frac{e^{-\lambda Z}}{J_o^2\left(A\sqrt{1+\lambda^2}\right) + Y_o^2\left(A\sqrt{1+\lambda^2}\right)}\, d\lambda \right) \qquad (52)$$

The behavior of these two integrals near Z = 0 has been discussed by Duncan [11]. The leading term, however, can easily be obtained by comparing Eq. (50) with Eq. (10). Since the asymptotic expressions of the two integrands in Eq. (50) and Eq. (10) behave exactly in the same manner as $\lambda \to \infty$ on the real axis, the leading term of $I_t(Z)$ in Eq. (50) will then be

$$I_t(Z) \sim \frac{i2VA}{\zeta_o} \ln \lambda_o Z \qquad \text{as } Z \to 0. \qquad (53)$$

Furthermore, we can actually prove that this logarithmic current exists only on the outer surface. That is, if we substitute Eqs. (6a, b), (48a, b) into Eq. (44), as $H \to \infty$,

$$A_Z(Z) = \frac{i}{4\nu_o} \int_C I_t(\lambda)\, H_o^{(1)}\left(R_> \sqrt{1-\lambda^2}\right) J_o\left(R_< \sqrt{1-\lambda^2}\right) e^{-i\lambda Z}\, d\lambda$$

$$+ \frac{A}{4\nu\zeta_o} \int_C \frac{1}{\sqrt{1-\lambda^2}} J_1\left(A\sqrt{1-\lambda^2}\right) H_o^{(1)}\left(R\sqrt{1-\lambda^2}\right) e^{-i\lambda Z}\, d\lambda \qquad (54)$$

where $R_{\gtrless} = \begin{matrix}\max \\ \min\end{matrix}\{R, A\}$. A comparison of (54) with Eq. (25), after the introduction of $I_{in}(\lambda)$ as the Fourier transform of $I_{in}(Z)$, leads to

$$I_{in}(\lambda) = \frac{-i\pi A}{2} I_t(\lambda) \sqrt{1-\lambda^2}\, H_o^{(1)}\left(A\sqrt{1-\lambda^2}\right) J_o\left(A\sqrt{1-\lambda^2}\right)$$

$$- \frac{\pi A^2}{2\zeta_o} V H_1^{(1)}\left(A\sqrt{1-\lambda^2}\right) J_1\left(A\sqrt{1-\lambda^2}\right). \qquad (55)$$

The substitution of Eq. (50) into Eq. (55) yields

$$I_{in}(\lambda) \equiv 0.$$

Therefore, $I_{in}(Z)$ vanishes everywhere in the case of the infinitely long antenna, and $I_{out}(Z)$ increases logarithmically near the origin.

B. NUMERICAL SOLUTION FOR THE CURRENT DISTRIBUTION

Let $D_K = D_o(Z_K; A)$. With Eq. (43), Eq. (46) leads to

$$\sum_{m=1}^{2N+1} \beta_{Km}^{(\iota)} I_m^{(t)} = \frac{i2\pi}{\zeta_o} V(\sin Z_K + D_K) \cdot \frac{1}{2} f_K^{(t)}, \quad K = 1, 2, \ldots 2N+1, \qquad (56)$$

where $\beta_{Km}^{(t)}$ and $f_K^{(t)}$ are defined in Eqs. (17) and (23), respectively.

In order to evaluate that part of the current which is distributed on the outside (inside) surface, an expression for the difference current can also be obtained by the previous method. However, in this case, the difference current also has a logarithmic singularity at the driving point.

By comparison with Eq. (25), the magnetic field now becomes

$$B_\theta(Z; R) = \frac{-k_o}{4\pi\nu_o} \frac{\partial}{\partial R} \int_{-H}^{+H} I_t(Z') K(Z-Z';R)\, dZ' + \frac{jk_o V}{2\nu_o\zeta_o} \frac{\partial}{\partial R} D_o(Z;R) \qquad (57)$$

Therefore,

$$I_d(Z) = 2\pi a \nu_o [B_\theta(Z; R=A+\epsilon) + B_\theta(Z; R=A-\epsilon)]$$

$$= -\frac{A}{2} \int_{-H}^{+H} I_t(Z') \left[\frac{\partial}{\partial R} K(Z-Z';R) \Big|_{R=A+\epsilon} + \frac{\partial}{\partial R} K(Z-Z';R) \Big|_{R=A-\epsilon} \right] dZ'$$

$$+ \frac{i\pi AV}{\zeta_o} \left[\frac{\partial}{\partial R} D_o(Z;R) \Big|_{R=A+\epsilon} + \frac{\partial}{\partial R} D_o(Z;R) \Big|_{R=A-\epsilon} \right];$$

$$\text{as } \epsilon \to 0 \text{ and } |Z| \leq H \qquad (58)$$

With the definition,

$$g(Z) = \frac{i\pi AV}{\zeta_o} \left\{ \left[\frac{\partial}{\partial R} D_o(Z;R) \Big|_{R=A+\epsilon} + \frac{\partial}{\partial R} D_o(Z;R) \Big|_{R=A-\epsilon} \right] - \frac{2}{\pi} \ln \frac{|Z|}{H} \right\};$$

$$\text{as } \epsilon \to 0 \text{ and } |Z| \leq H \qquad (59)$$

and $g_K = g(Z_K)$, Eq. (58) can be transformed into

$$I_K^{(d)} = \sum_{m=1}^{2N} \beta_{Km}^{(d)} I_m^{(t)} + \frac{1}{2} f_K^{(d)} + g_K + \frac{i2AV}{\zeta_o} \ln \frac{(K-1)\Delta}{H}; \quad K = 1, 2, \ldots 2N+1 \qquad (60)$$

where $\beta_{Km}^{(d)}$ and $f_K^{(d)}$ are defined in Eqs. (28) and (29). The second term in Eq. (59) is added so that g_K is finite for all K.

C. EVALUATION OF D_K AND g_K

From Eqs. (48a, b),

$$D_K = \frac{iA}{2} \int_C \frac{1}{\sqrt{1-\lambda^2}} J_1\left(A\sqrt{1-\lambda^2}\right) H_o^{(1)}\left(A\sqrt{1-\lambda^2}\right) e^{-i\lambda K\Delta} d\lambda \qquad (61)$$

Aside from the logarithmic singularities at the branch points, the integrand has no other singularity. Also, as $|\lambda| \to \infty$ in the lower half plane,

$$\frac{e^{-i\lambda K\Delta}}{\sqrt{1-\lambda^2}} J_1\left(A\sqrt{1-\lambda^2}\right) H_o^{(1)}\left(A\sqrt{1-\lambda^2}\right) \sim \text{const}\,\frac{1}{\lambda^2}\, e^{-K\Delta\left|I_m\lambda\right|} \tag{62}$$

so that the contour can be deformed from C to C';

$$D_K = \frac{iA}{2}\left\{\left(\int_{-i\infty}^{0} + \int_{0}^{-1}\right)\frac{e^{-i\lambda K\Delta}}{e^{+i\pi}\left|\sqrt{\lambda^2-1}\right|} J_1\left(A\, e^{+i\pi}\left|\sqrt{\lambda^2-1}\right|\right)\right.$$

$$\cdot H_o^{(1)}\left(A\, e^{+i\pi}\left|\sqrt{\lambda^2-1}\right|\right)\, d\lambda$$

$$+ \left(\int_{-1}^{0} + \int_{0}^{-i\infty}\right)\frac{e^{-i\lambda K\Delta}}{\left|\sqrt{\lambda^2-1}\right|} J_1\left(A\left|\sqrt{\lambda^2-1}\right|\right)$$

$$\left.\cdot H_o^{(1)}\left(A\left|\sqrt{\lambda^2-1}\right|\right)\, d\lambda\right\}$$

$$= iA\int_0^1 \frac{e^{+iK\Delta\lambda}}{\sqrt{1-\lambda^2}} J_o\left(A\sqrt{1-\lambda^2}\right) J_1\left(A\sqrt{1-\lambda^2}\right)$$

$$+ A\int_0^\infty \frac{1}{\sqrt{1+\lambda^2}} J_o\left(A\sqrt{1+\lambda^2}\right) J_1\left(A\sqrt{1+\lambda^2}\right) e^{-\lambda K\Delta}\, d\lambda \tag{63}$$

As for the evaluation of g_K, first, define $L(Z) = \frac{2}{\pi}\ln\frac{|Z|}{H}$ for $|Z| \leq H$ and $L(Z) = 0$ for $|Z| > H$. Then the Fourier transform of $L(Z)$ is

$$L(\lambda) = \frac{1}{2\pi}\int_{-\infty}^{+\infty} L(Z)\, e^{+i\lambda Z}\, dZ$$

$$= \frac{1}{\pi}\int_0^H \ln\frac{Z}{H}\cos\lambda Z\, dZ$$

$$= -\frac{S_i(\lambda H)}{\pi\lambda} \tag{64a}$$

and

$$L(Z) = \int_C L(\lambda)\, e^{-i\lambda Z}\, d\lambda. \tag{64b}$$

Here, $Si(\lambda H)$ is the sine integral whose behavior at $\lambda \to \infty$ is known. It is

$$Si(\lambda H) \sim \frac{\pi}{2} - \frac{1}{\lambda H} \cos \lambda H. \tag{65}$$

Now substitute Eqs. (64a, b), (48a, b) into Eq. (59) to obtain:

$$g_K = \frac{i\pi AV}{\zeta_o} \int_C (-iA) \left[J_1\left(A\sqrt{1-\lambda^2}\right) H_1^{(1)}\left(A\sqrt{1-\lambda^2}\right) + \frac{i2}{\pi^2 A} \frac{Si(\lambda H)}{\lambda} \right] e^{-i\lambda(K-1)\Delta}\, d\lambda \tag{66}$$

as $\lambda \to \infty$ on the real axis,

$$\left[J_1\left(A\sqrt{1-\lambda^2}\right) H_1^{(1)}\left(A\sqrt{1-\lambda^2}\right) + \frac{i2}{\pi^2 A} \frac{Si(\lambda H)}{\lambda} \right] e^{-i\lambda K\Delta}$$

$$\sim e^{-i\lambda K\Delta} \left\{ \left[\frac{-i}{\pi A\lambda} + \frac{i2}{\pi^2 A} \left(\frac{\pi}{2\lambda}\right) \right] + 0\left(\frac{1}{\lambda^2}\right) \right\}$$

$$\sim \text{const}\, \frac{e^{-i\lambda(K-1)\Delta}}{\lambda^2}. \tag{67}$$

However, since $Si(\lambda H)$ increases exponentially along the imaginary axis, Eq. (58) is not true on both sides of the branch cut, and the integration has to be performed on the real axis.

$$g_K = \frac{2\pi A^2 V}{\zeta_o}\left\{\int_0^1 \left[J_1\left(A\sqrt{1-\lambda^2}\right) H_1^{(1)}\left(A\sqrt{1-\lambda^2}\right) + \frac{i2}{\pi^2 A}\frac{Si(\lambda H)}{\lambda}\right] \cos\lambda(K-1)\Delta\, d\lambda\right.$$

$$\left. - \frac{i2}{\pi}\int_1^\infty \left[I_1\left(A\sqrt{\lambda^2-1}\right) K_1\left(A\sqrt{\lambda^2-1}\right) - \frac{1}{\pi A}\frac{Si(\lambda H)}{\lambda}\right] \cos\lambda(K-1)\Delta\, d\lambda\right\} \tag{68}$$

Here, g_K is indeed of the order of A^2. Therefore, aside from the driving point, $I_K^{(d)}$ in Eq. (60) is equivalent to $I_K^{(d)}$ in Eq. (30), in the case of thin antennas.

IV. NUMERICAL RESULTS

Based upon Eqs. (24), (27), (56), and (58), a numerical solution for the current distributions along antennas with various radii and heights can be obtained for both 1-sided and 2-sided excitation. Also, the input conductance of the antenna is readily known as the real part of the total current at the driving point, in the case of 2-sided excitation and that of the outside current in the case of 1-sided excitation. The input susceptance of the antenna, however, is always infinite in either case, due to the fact that the singular current near the driving point is purely imaginary.

Also, in the process of numerical computation, the choice of the number of sample points depends upon the accuracy required for the solution on the one hand, and the computation time on the other. As a compromise, a less elegant method is adopted. That is, the antenna height is first divided into N segments (thus, 2N+1 sample points), and a set of solutions is obtained at these sample points. Then, the number of segments is doubled and another set is obtained. N is required to be large enough so that the difference between these two sets is less than 1-2%. In this manner although it is not known exactly how this approximate solution converges to the true solution, at least a self-consistent one is obtained.

Accordingly, numerical data for antennas with radii ranging from $\frac{a}{\lambda} = 0.03907$ to 0.5, and antenna heights ranging from $\frac{h}{\lambda} = 0.1$ to 0.5 have been obtained. For antennas with radii $\frac{a}{\lambda} < 0.16$, the input conductances vs. antenna heights are compared with the experimental data obtained

by Holly [12]. For antennas with larger radii, no experimental data are yet available.

A. CURRENT DISTRIBUTION

1. Half-Wavelength Antenna with 2-Sided Excitation

Current distributions for $\frac{1}{2}\lambda$-antennas with 2-sided excitation are shown in Figs. (4a)-(4i). The real part of the total current $I_T(Z)$ behaves very much like a combination of terms made up of cosines and shifted cosines with half-angle arguments, except near the ends of the antenna where the slope is larger than given by these two terms. This sharp increase in slope can be interpreted as a consequence of an extremely large accumulation of charge at the ends of the antenna. Furthermore, the accumulated charges are distributed on both inside and outside surfaces of the tubular antenna; they are proportional to the slopes of the real parts of the outside and inside currents, respectively. The imaginary part of the total current, on the other hand, can be approximated by trigonometric functions only after the subtraction of a logarithmic term. Also, the slope of this part at the ends is less than that of the real part in most cases. It follows that the predominant part of the charge accumulation is proportional to the time rate of change of the real part of the current, with which it is in phase quadrature.

For an antenna with a radius less than the cutoff wavelength of the lowest waveguide mode (i.e., $\lambda_{TM_{01}}$), the real part of the outside current can be approximated by a combination of cosine and shifted half-cosine terms with an argument of $k_o(z+\epsilon)$, where ϵ is a certain number

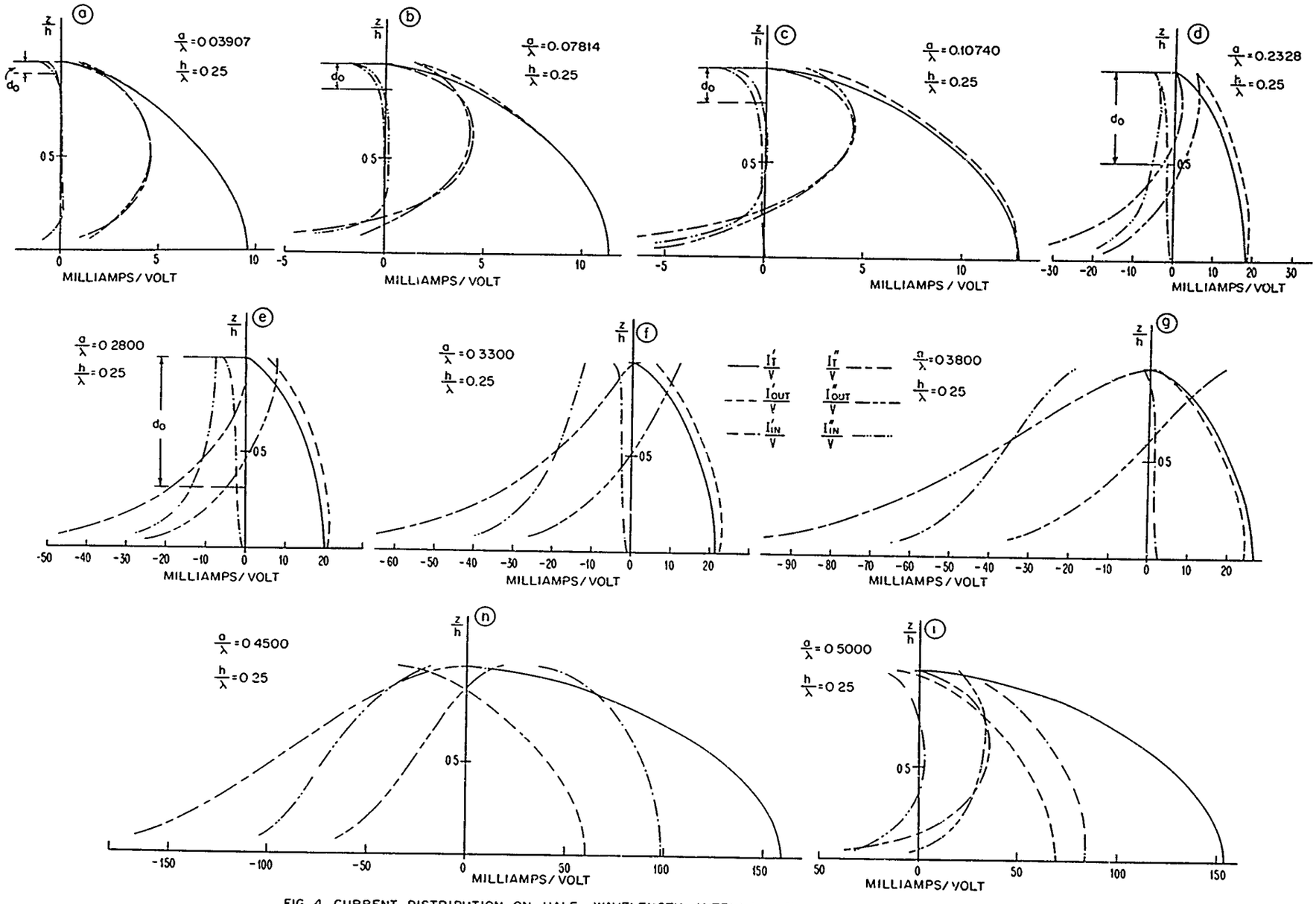

FIG 4 CURRENT DISTRIBUTION ON HALF-WAVELENGTH ANTENNA WITH 2-SIDES EXCITATION

which has the physical interpretation of an "end correction." At the end of the antenna, this real part of $I_{out}(Z)$ remains finite and reverses its direction as the current passes around the edge of the cylinder from the outside surface to the inside surface of the antenna. Once inside, it decreases toward the driven point. The rate of this decrease is, in general, comparable to, but certainly not the same as that of the TM_{01} mode, since other higher modes also exist near the end. As indicated in the figures, α_o is the "skin-depth" of the TM_{01} mode where the corresponding current decays $\frac{1}{e}$ of its value at the end. As $\frac{a}{\lambda}$ becomes larger, the attenuation decreases. Also, from the viewpoint of the inside generator, as the radius of the "waveguide" (i.e., the inside of the antenna) becomes larger, radiation due to the open ends increases. Thus at $\frac{a}{\lambda} = 0.38$ which is barely under the cutoff wavelength, the inside generator actually contributes to the radiated power, as the real part of the inside current becomes positive at the driving points.

On the other hand, for half-wave antennas with smaller radius $\left(\frac{a}{\lambda} \lesssim 0.04\right)$ the imaginary part of the outside current is inductive along most of the antenna, except in the region near the driving point where it is capacitive with a logarithmic singularity. At the end of the antenna, it has a finite inductive value on the outside surface. As it changes direction it becomes a capacitive current on the inside surface, where it decreases very rapidly toward the driving point, where the capacitive logarithmic current becomes dominant again. Thus, the total current distribution along half-wave dipoles that are not too thick is mostly

inductive.* As $\frac{a}{\lambda}$ becomes larger, the range over which the imaginary part of the total current is inductive is reduced; at $\frac{a}{\lambda} = 0.38$, it becomes totally capacitive. At the same time, the region on the inner surface of the tube in which the imaginary part of the current decreases toward the driving point disappears completely.

For an antenna with a radius larger than $\lambda_{TM_{01}}$, the inside generator begins to play an active role. The real part of the current on the inside surface, instead of having a maximum at the end of the antenna and decreasing toward the driving point, now increases toward the generator and reaches the maximum at the driving point. The imaginary part of the current on the inner surface of the antenna, on the other hand, is capacitive when $\frac{a}{\lambda} = 0.45$ and inductive when $\frac{a}{\lambda} = 0.50$. As will be shown later in section C, the half-wavelength antenna is not yet resonant when $\frac{a}{\lambda} = 0.45$, but it has passed through resonance when $\frac{a}{\lambda} = 0.50$. In either case, the magnitudes of both the real and imaginary parts of the current on the inner surface of the antenna are larger than their counterparts on the outside.

2. Half-Wavelength Antenna with One-sided Excitation

Current distributions for $\frac{1}{2}\lambda$-antennas with 1-sided excitation are shown in Figs. (5a)-(5i). For antennas with radii less than $\lambda_{TM_{01}}$, the real part of both inside and outside currents behave very much the same as with 2-sided excitation. At $\frac{a}{\lambda} = 0.38$, the real part of the current

---

*Inductive in the sense that the region where the imaginary current is inductive is much larger than the region which is capacitive. Of course, in any case, the input susceptance is always capacitive.

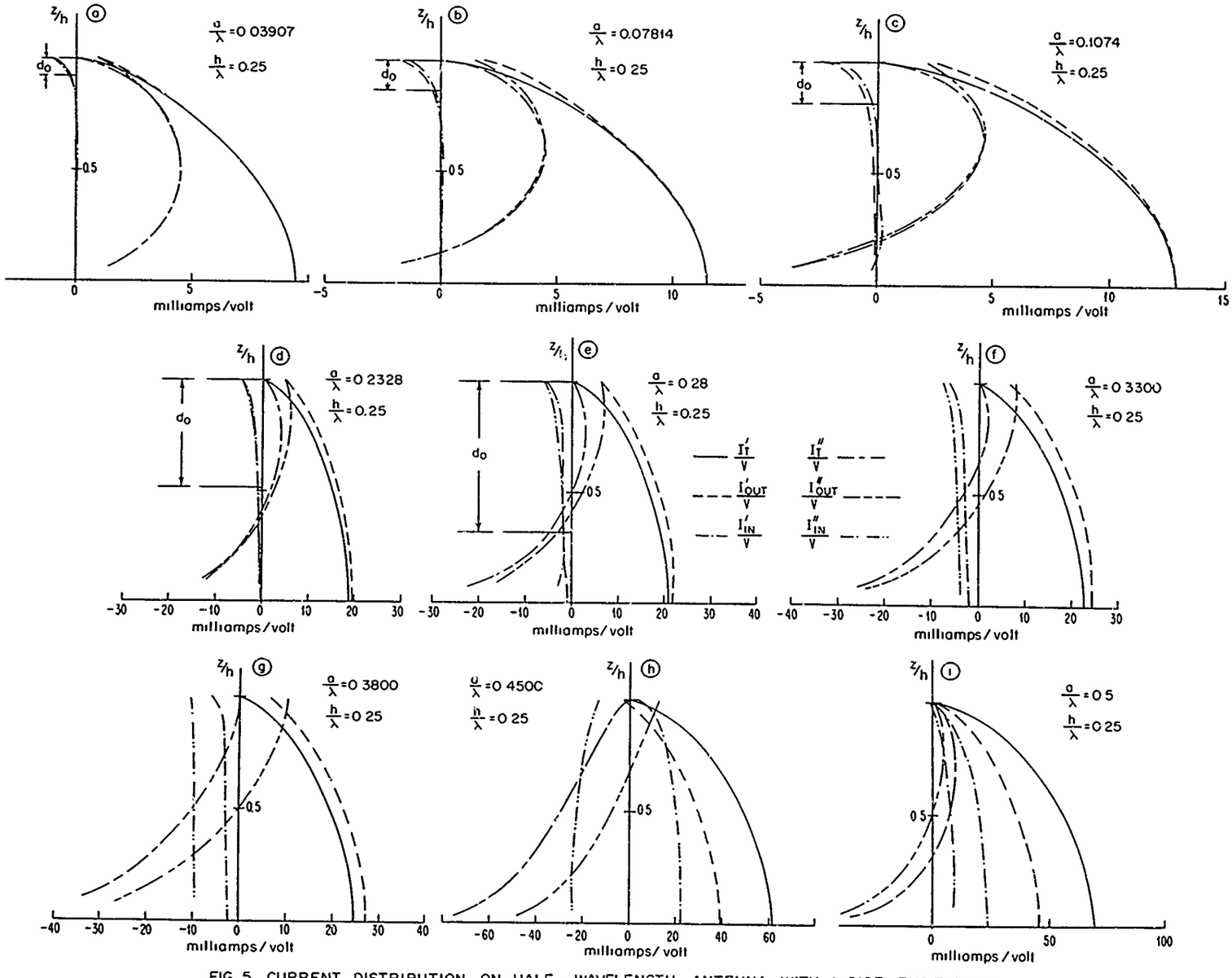

FIG 5 CURRENT DISTRIBUTION ON HALF - WAVELENGTH ANTENNA WITH 1-SIDE EXCITATION

remains negative everywhere on the inside surface of the antenna, instead of becoming positive near the driving point as it does with 2-sided excitation. This reveals that the inside generator actively delivers power even though the interior of the tube is still well under the cutoff of the lowest waveguide mode.

The imaginary part of the current with 1-sided excitation is noticeably different from that with a 2-sided generator. Specifically, on the inner surface, this current is finite everywhere. There is, of course, no discontinuity due to a generator at Z = 0 on the inside surface.

For an antenna with a radius larger than $\lambda_{TM_{01}}$, the magnitudes of both the real and imaginary parts of the current on the inside of the antenna increase toward the generator and reach a maximum at the driving point. Also, the phase relationship between the real and imaginary parts of the current remains constant along the antenna (except in the region near the end), since they both form the standing-wave pattern characteristic of a short-circuited waveguide.

3. Full Wavelength Antenna with Two-sided Excitation

Current distributions for the full wavelength-antenna with 2-sided excitation are shown in Figs. (6a)-(6g). The real part of the total current, in this case, can still be approximated by a shifted cosine and a shifted cosine with half-angle argument, while the imaginary part can be approximated by the trigonometric functions only after the subtraction of a logarithmic term. Near the end of the antenna, the slope of the real part of the current is now less than that of the imaginary part. Therefore the charge accumulation near the end is predominantly real.

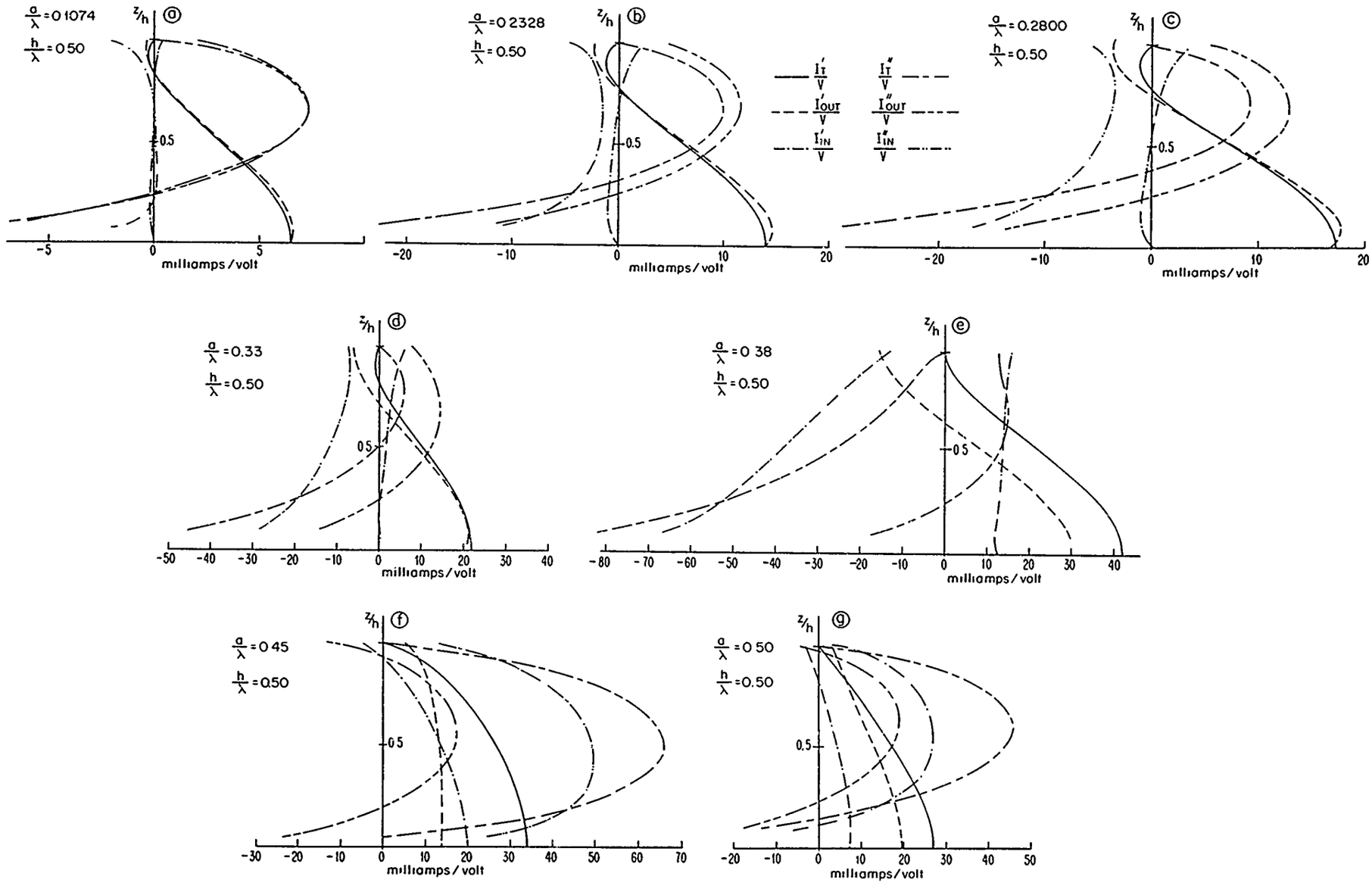

FIG 6 CURRENT DISTRIBUTION ON FULL - WAVELENGTH ANTENNA WITH 2-SIDES EXCITATION

For an antenna with a radius less than $\lambda_{TM_{01}}$, the real part of the current on the outer surface of the antenna can be approximated in a fashion similar to that for a $\frac{1}{2}\lambda$-antenna. However, owing to the length of the antenna, this real part of the current now is negative at the end. On the inner surface, the real part of the current decreases rapidly and there exists a region where it has a small but negative value. At the driving point, however, it is very close to zero and, hence, is negligible compared to its counterpart on the outside surface. As $\frac{a}{\lambda}$ increases, this region with a small negative value decreases and the real current on the inside surface becomes more and more positive. At $\frac{a}{\lambda} = 0.38$, it has a large positive value everywhere inside the antenna, and the inside generator again contributes significantly to the radiated power. Also, as $\frac{a}{\lambda}$ increases, the imaginary part of the total current changes from mostly inductive to purely capacitive, while the current on the outer surface remains inductive and is not sensitive to an increase in $\frac{a}{\lambda}$.

For an antenna with radius larger than $\lambda_{TM_{01}}$, the inside generator again plays an active role. The real part of the current on the inside surface now has a maximum at the driving point, decreasing toward the end, where it becomes negative. Also, unlike the situation in the $\frac{1}{2}\lambda$-antenna, the imaginary part of the current on the inside surface is mostly inductive for $\frac{a}{\lambda} = 0.45$ and 0.50. This is a consequence of the fact that the antenna is very much longer than resonant.

4. Full-Wavelength Antenna with One-sided Excitation

Current distributions for the λ-antenna with 1-sided excitation are shown in Figs. (7a)-(7g). Similar to the case of the $\frac{1}{2}\lambda$-antenna, the

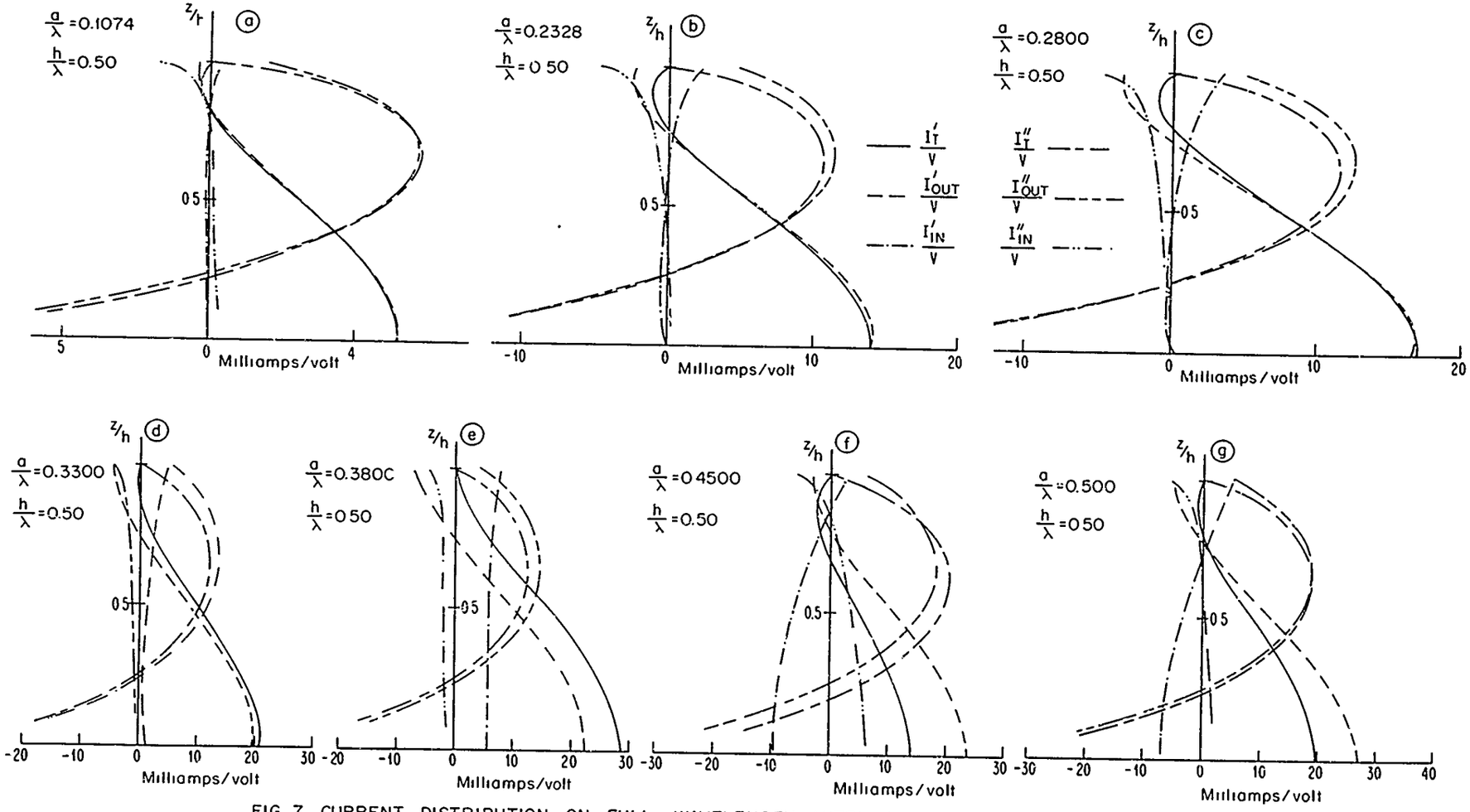

FIG 7 CURRENT DISTRIBUTION ON FULL - WAVELENGTH ANTENNA WITH 1-SIDE EXCITATION

distribution of the real part of the current behaves very much like that with the 1-sided excitation, when $\frac{a}{\lambda}$ is less than $\lambda_{TM_{01}}$, and the imaginary current has no logarithmic term on the inside surface. For $\frac{a}{\lambda}$ larger than $\lambda_{TM_{01}}$, away from the end of the antenna both real and imaginary parts of the current on the inner surface follow the same standing-wave pattern. The phase relation between these two components of current also remains constant along the antenna.

B. INPUT CONDUCTANCE

The input conductance of an antenna with various values of radius vs. the antenna height are shown in Figs. (8a)-(8c). For convenience in the description, let the whole antenna be treated as consisting of two coupled radiating systems: system ① is driven by the generator on the outside surface; system ② by the generator on the inside. The two systems are then coupled by way of the open end of the antenna. Thus, currents and voltages at the two driving points can be related by the equation

$$\begin{cases} I_1 = Y_{11}V_1 + Y_{12}V_2 \\ \\ I_2 = Y_{21}V_1 + Y_{22}V_2 \end{cases} \tag{69}$$

where Y_{11} and Y_{22} are the self-admittances of systems ① and ②, respectively, and Y_{12} and Y_{21} are the mutual admittances. The input conductances G_1 and G_2 of an antenna with 1-sided and 2-sided excitation are given, respectively, by

$$\begin{cases} G^{(1)} = \text{Real part of } Y_{11} = G_{11} \\ G^{(2)} = \text{Real part of } (Y_{11}+Y_{22}+Y_{12}+Y_{21}) = G_{11}+G_{22}+G_{12}+G_{22} \end{cases} \tag{70}$$

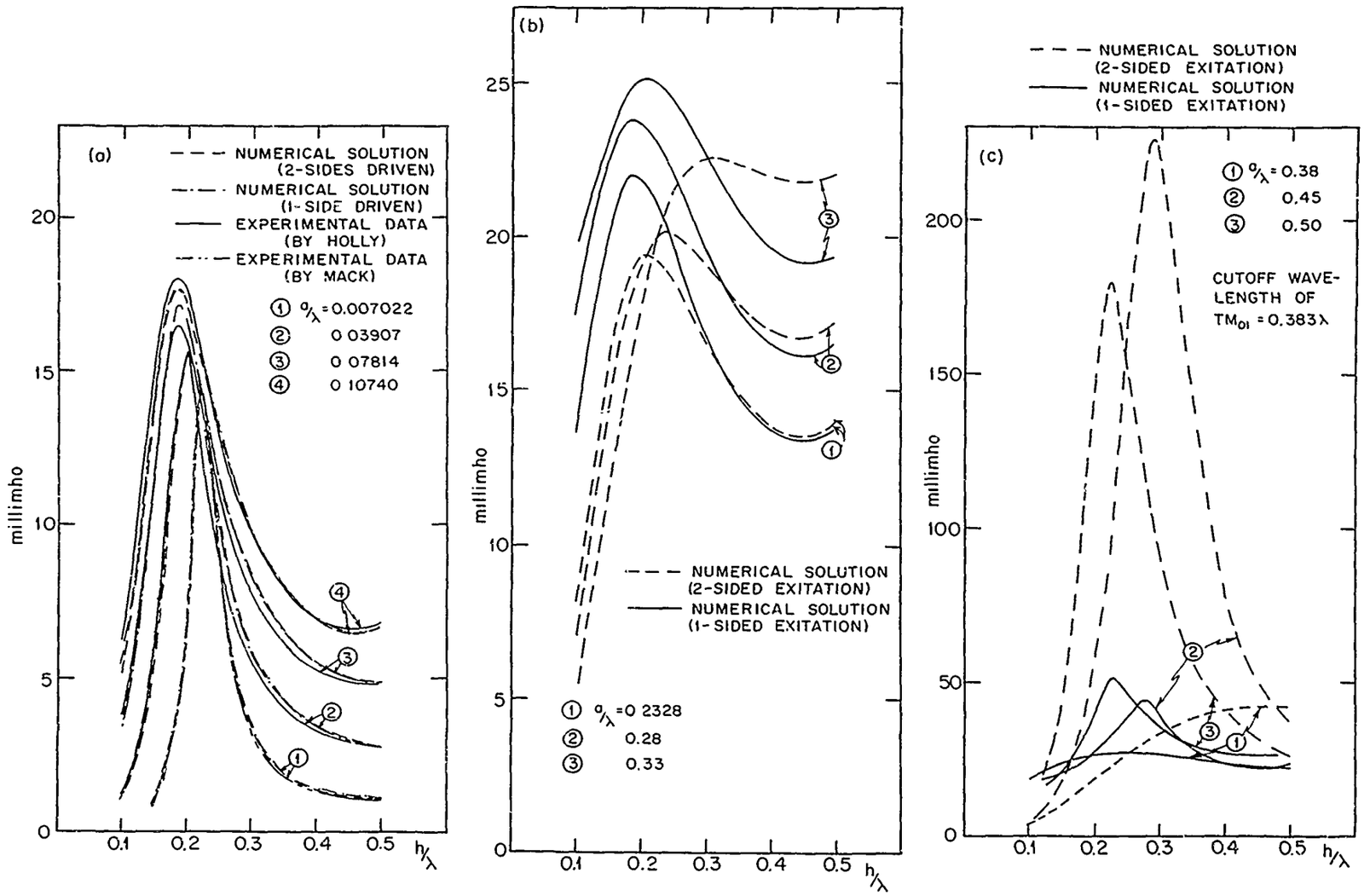

FIG. 8 INPUT CONDUCTANCE VS. ANTENNA HEIGHT

(1) Antenna with moderately large radius $\left(\frac{a}{\lambda} < 0.16 \text{ or } 2\pi a < \lambda,\right.$ i.e., the circumference of the antenna is less than a wavelength$\left.\right)$:

For antennas in this range, the radius is much smaller than the cutoff wavelength of the TM_{01} waveguide mode, even though it may be very large compared to the conventional dipole antenna. Therefore, the input conductance is not sensitive to the method of excitation (i.e., $G_{11} \gg G_{12}, G_{22}$). The general behavior of the input conductance vs. antenna height is also similar to that of the conventional thin antenna. As $\frac{a}{\lambda}$ is increased, both values of the input conductance at resonance* (G_{max}) and antiresonance (G_{min}) increase, but the ratio of the two decreases. Also, the resonant and the antiresonant lengths decrease. Thus, the corresponding curve in Fig. (8a) will move up, shift toward the left and become flatter.

Data obtained from the numerical solution are in good agreement with those obtained experimentally by Mack [13], in the case of conventional thin antennas. For antennas with moderate large radii $\left(\frac{a}{\lambda} \geq 0.03907\right)$, the agreement with data obtained by Holly [12] is also reasonably good. The two curves seem to differ by less than $0.0075\,\lambda$, and the experimental value at resonance is consistently less than the numerical solution by only 3-4%. (For $\frac{a}{\lambda} = 0.01074$, the comparison is actually based on an average experimental value of $\frac{a}{\lambda} = 0.10157$ and $\frac{a}{\lambda} = 0.11287$, therefore is less accurate.)

(2) Antenna with radius less than $\lambda_{TM_{01}}$ $(0.16 < \frac{a}{\lambda} < 0.383)$:

As the radius of the antenna becomes larger, the difference between

---

*Resonance (or antiresonance) is defined as the position where the input conductance reaches maximum (or minimum).

the input conductance with 1-sided and 2-sided excitations also becomes more significant. For a fixed radius, the corresponding curve for $G^{(1)}$ becomes sharper than that of $G^{(2)}$. Also, it has a larger resonant conductance, but smaller antiresonant conductance. The resonant lengths for the two different excitations are different, too, since the behavior of G_{11} is no longer approximately the same as $(G_{11}+G_{12}+G_{21}+G_{22})$. Furthermore, when the antenna is short, the coupling between the inside and the outside surfaces is comparatively stronger, and the real part of the current on the inner surface is negative at the driven point. When the antenna is long, the coupling is comparatively weaker, and the real part of the current on the inner surface is positive at the driven point. Therefore, $G^{(1)}$ is quite a bit larger than $G^{(2)}$ when the antenna is short, and is a little smaller than $G^{(2)}$ when the antenna is long.

As the radius of the antenna is increased, both the input conductances at resonance $G^{(1)}_{max}$ (or $G^{(2)}_{max}$) and at antiresonance $G^{(1)}_{min}$ (or $G^{(2)}_{min}$) become larger. However, the resonant lengths now increase and the antiresonant lengths remain relatively unchanged.

The behavior of $G^{(1)}$ and $G^{(2)}$ near resonance and antiresonance, and also the location of resonance as a function of $\frac{a}{\lambda}$ are shown in Fig. 9.

(3) Antenna with radius larger than $\lambda_{TM_{01}}$ $\left(\frac{a}{\lambda} > 0.383\right)$:

Since the TM_{01} mode can now propagate in the inside of the antenna, both $G^{(1)}$ and $G^{(2)}$ reach a sharp maximum when this waveguide mode is at resonance. However, for a fixed radius, the value of $G^{(2)}_{max}$ is much larger than that of $G^{(1)}_{max}$. This is due to the fact that the TM_{01} mode is driven at the location of the maximum current with 2-sided excitation, but excited only by the coupling from the outside at the end of the antenna with 1-sided excitation.

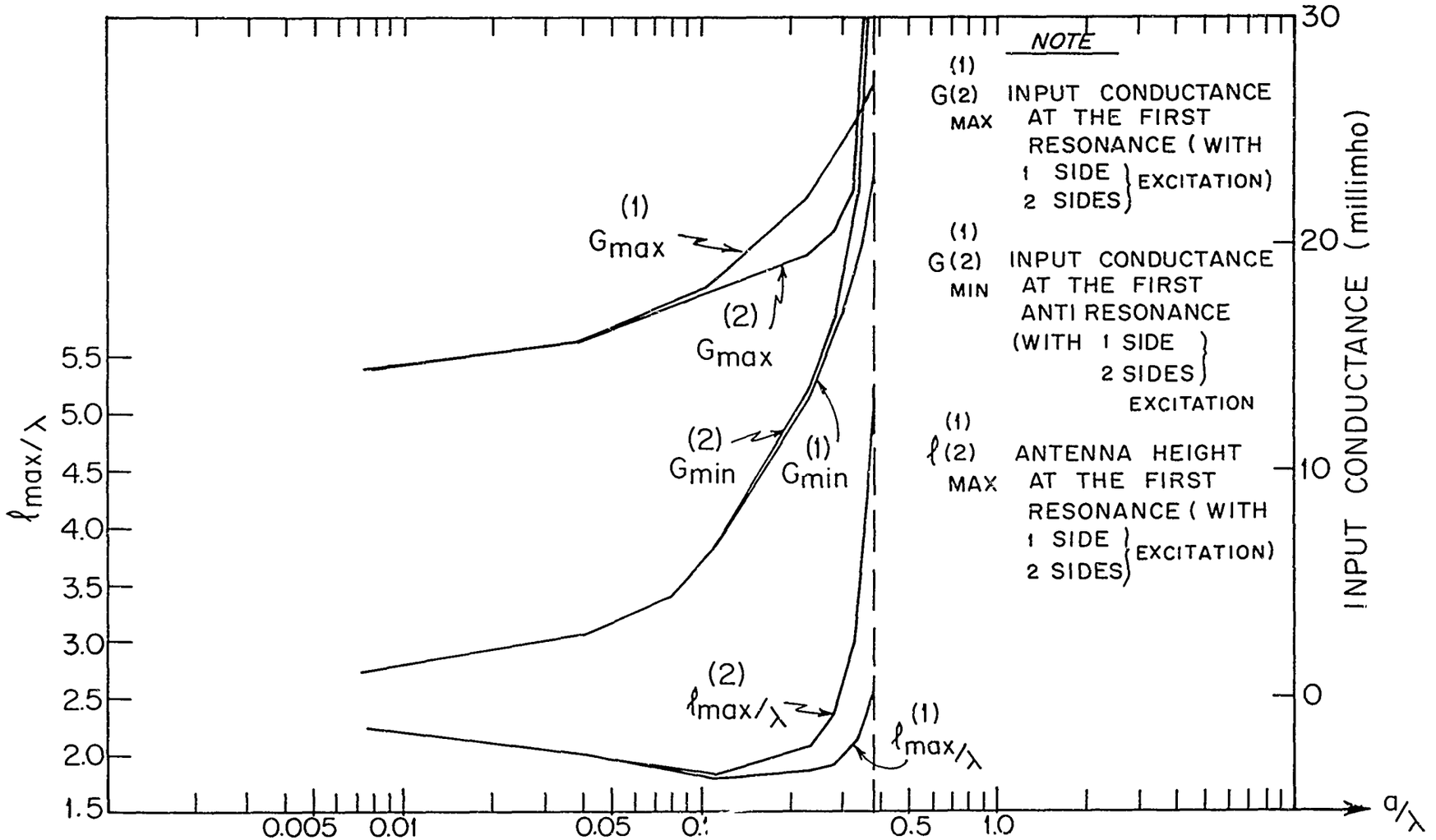

FIG. 9. INPUT CONDUCTANCE AND ANTENNA HEIGHT AT RESONANCE vs. a/λ

V. CONCLUSION

The problem of the thick dipole antenna has been investigated theoretically for both 1-sided and 2-sided excitations. When the circumference of the antenna is less than one wavelength, the solution obtained from the physically more realizable model with 1-sided excitation does not differ significantly from the conventional model with 2-sided excitation. However, for antennas with larger radius, it is only correct to use the model with 1-sided excitation in order to obtain a solution that is comparable with measured results.

REFERENCES

1. R. W. P. King, The Theory of Linear Antennas, Harvard University Press, Cambridge, Mass. (1956), p. 76.

2. R. W. P. King, The Theory of Linear Antennas, Harvard University Press, Cambridge, Mass. (1956), pp. 101-110.

3. C. T. Tai, "A Variational Solution to the Problem of Cylindrical Antennas," Technical Report No. 12, SRI Project No. 188, Stanford Research Institute, August 1950.

4. R. W. P. King, "Linear Arrays: Currents, Impedances and Fields," Trans. IRE AP-7, December 1959.

   R. W. P. King and T. T. Wu, "Currents, Charges, and Near Fields of Cylindrical Antennas," Technical Report No. 466, Cruft Laboratory, Harvard University, April 1965.

5. T. T. Wu, "Theory of the Dipole Antenna and Two-Wire Transmission Line," Technical Report No. 318, Cruft Laboratory, Harvard University, March 1960.

6. R. H. Duncan and F. A. Hinchey, "Cylindrical Antenna Theory," Journal of Research NBS 64D, Radio Propagation, No. 5, pp. 569-584, 1960.

7. K. K. Mei, "On the Integral Equations of Thin Wire Antennas," PGAP, AP-13, pp. 374-378, April 1965.

8. T. T. Wu and R. W. P. King, "The Integral Equation for the Current in a Thick Tubular Antenna," Technical Report No. 502, Cruft Laboratory, Harvard University, May 1966.

9. T. T. Wu and R. W. P. King, "Driving Point and Input Admittance of Linear Antennas," Journal of Applied Physics 30, pp. 74-76, 1959.

10. A. Young, "The Application of Approximate Product-Integration to the Numerical Solution of Integral Equations," Cambridge Philosophical Society, Vol. 224, pp. 552-573, April 1954.

11. R. H. Duncan, "Theory of the Infinite Cylindrical Antenna Including the Feedpoint Singularity in Antenna Current," Journal of Research NBS Vol. 66D, No. 2, pp. 181-187, April 1962.

12. S. Holly, Private communication.

ACKNOWLEDGEMENT

The author wishes to express his deepest appreciation to Professors R. W. P. King and T. T. Wu for their guidance and encouragement. He also wishes to thank Mr. C. Y. Ting for numerous suggestions and discussions.

BLANK PAGE

APPENDIX

Define

$$P(m,\lambda) = \lambda \int_{-2\Delta}^{+2\Delta} \ln \left|\frac{Z'}{2\Delta}\right| e^{-i|m\Delta - Z'|\lambda}\, dZ'$$

$$P(0,\lambda) = 2\lambda \int_0^{2\Delta} \ln \frac{Z'}{2\Delta}\, e^{-iZ'\lambda}\, dZ'$$

$$= 2i\left[\ln \frac{Z'}{2\Delta}\,(e^{-iZ'\lambda} - 1)\,\Big|_0^{2\Delta} - \int_0^{2\Delta} \frac{e^{-iZ'\lambda} - 1}{Z'}\, dZ'\right]$$

$$= -2i[Ci(2\lambda\Delta) - \nu - \ln 2\lambda\Delta + iSi(2\lambda\Delta)] \qquad (A\text{-}1)$$

$$P(1,\lambda) = \lambda \int_{-2\Delta}^{\Delta} \ln \left|\frac{Z'}{2\Delta}\right| e^{-i(\Delta - Z')\lambda}\, dZ' + \lambda \int_{\Delta}^{2\Delta} \ln \frac{Z'}{2\Delta}\, e^{+i(\Delta - Z')\lambda}$$

$$= 2\lambda \cos \lambda\Delta \int_0^{2\Delta} \ln \frac{Z'}{2\Delta}\, e^{-iZ'\lambda}\, d\lambda + i2\lambda \int_0^{\Delta} \ln \frac{Z'}{2\Delta} \sin (Z' - \Delta)\lambda\, dZ'$$

$$= \frac{2\lambda\Delta}{i}[Ci(2\lambda\Delta) - \nu - \ln 2\lambda\Delta - iSi(2\lambda\Delta)]$$

$$+ 2i\lambda\left[-\frac{\cos \Delta\lambda}{\lambda} \int_0^{\Delta} \ln \frac{Z'}{\Delta}\, d(\cos \lambda Z' - 1) - \frac{\sin \Delta\lambda}{\lambda} \int_0^{\Delta} \ln \frac{Z'}{\Delta}\, d \sin Z'\lambda\right.$$

$$\left. + \frac{\ln 2}{\lambda} \cos (Z' - \Delta)\lambda \,\Big|_0^{\Delta}\right]$$

$$= 2i\{\cos \lambda\Delta[-Ci(2\lambda\Delta) + Ci(\lambda\Delta) + iSi(2\lambda\Delta)] + \sin \lambda\Delta Si(\Delta\lambda) + \ln 2\} \qquad (A\text{-}2)$$

$$P(m,\lambda) = \lambda \int_0^{2\Delta} \ln \frac{Z'}{2\Delta}\,[e^{-i(m\Delta - Z')\lambda} + e^{-i(m\Delta + Z')\lambda}]\, dZ'$$

$$= 2e^{-im\Delta\lambda} \int_0^{2\Delta} \ln \frac{Z'}{2\Delta}\, d \sin Z'\lambda$$

$$= -2e^{-im\Delta\lambda}\, Si(2\Delta\lambda); \qquad m \geq 2, \qquad (A\text{-}3)$$

where Ci(Z), Si(Z) are the cosine and sine integrals, respectively. Substitute Eqs. (A-1, -2, -3) into Eqs. (17), (29) and compare with Eqs. (39) and (43):

$$f_K^{(t)} = \frac{iA}{30\pi}\left[i\int_0^i \frac{P(m,-\lambda)}{-\lambda} J_o^2\left(A\sqrt{i-\lambda^2}\right) d\lambda + \int_0^\infty \frac{P(m,-i\lambda)}{-i\lambda} J_o^2\left(A\sqrt{1+\lambda^2}\right) d\lambda \right] \tag{A-4}$$

$$\begin{aligned} f_K^{(d)} = {} & \frac{-A^2}{120\pi}\int_0^1 \frac{P(m,\lambda)-P(m,-\lambda)}{\lambda}\left[H_1^{(1)}\left(A\sqrt{1-\lambda^2}\right) J_o\left(A\sqrt{1-\lambda^2}\right)\right. \\ & \left. + H_o^{(1)}\left(A\sqrt{1-\lambda^2}\right) J_1\left(A\sqrt{1-\lambda^2}\right)\right] \sqrt{1-\lambda^2}\, d\lambda \\ & + \frac{iA^2}{30\pi}\int_0^\infty \frac{P(m,\lambda)-P(m,-\lambda)}{\lambda}\left[K_1\left(A\sqrt{1-\lambda^2}\right) I_o\left(A\sqrt{1-\lambda^2}\right)\right. \\ & \left. - K_o\left(A\sqrt{1-\lambda^2}\right) I_1\left(A\sqrt{1-\lambda^2}\right)\right] \sqrt{1-\lambda^2}\, d\lambda. \end{aligned} \tag{A-5}$$

ν in (A-1) is the Euler's constant.

Unclassified

Security Classification

DOCUMENT CONTROL DATA - R&D

(Security classification of title, body of abstract and indexing annotation must be entered when the overall report is classified)

1 ORIGINATING ACTIVITY (Corporate author) Cruft Laboratory Division of Engineering and Applied Physics	2a. REPORT SECURITY CLASSIFICATION Unclassified 2b GROUP

3. REPORT TITLE

ON THE ELECTRICALLY THICK CYLINDRICAL ANTENNA

4 DESCRIPTIVE NOTES (Type of report and inclusive dates)

Interim technical report

5 AUTHOR(S) (Last name, first name, initial)

Chang, David C.

6. REPORT DATE	7a. TOTAL NO. OF PAGES	7b. NO. OF REFS
August, 1966	44	12

8a. CONTRACT OR GRANT NO. Nonr-1866(32) b PROJECT NO. NR-371-016 c. d.	9a ORIGINATOR'S REPORT NUMBER(S) Technical Report No. 509 9b. OTHER REPORT NO(S) (Any other numbers that may be assigned this report)

10. AVAILABILITY/LIMITATION NOTICES

"Reproduction in whole or in part is permitted by the U. S. Government. Distribution of this document is unlimited.

11. SUPPLEMENTARY NOTES	12. SPONSORING MILITARY ACTIVITY
	Office of Naval Research

13. ABSTRACT

The problem of a thick cylindrical antenna driven by a "delta-function generator" is investigated. Numerical solutions are obtained for two different mathematical models - one is driven by a "delta-function generator" on both outside and inside surfaces of the antenna, and another is driven only on the outside surface. In both cases, current singularity near the driven point has been taken care of and subsequently subtracted out, before the numerical solution is applied. For antennas with circumferences less than a free-space wavelength, the results are compared with the experimental data obtained by Holly [12]. For antennas with larger radii, no experimental data are yet available.

DD FORM 1 JAN 64 1473

Unclassified

Security Classification

14. KEY WORDS	LINK A		LINK B		LINK C	
	ROLE	WT	ROLE	WT	ROLE	WT
electrically thick antenna numerical method input admittance current distribution ---on the inner surface ---on the outer surface resonance length						

INSTRUCTIONS

1. ORIGINATING ACTIVITY: Enter the name and address of the contractor, subcontractor, grantee, Department of Defense activity or other organization *(corporate author)* issuing the report.

2*a*. REPORT SECURITY CLASSIFICATION: Enter the overall security classification of the report. Indicate whether "Restricted Data" is included. Marking is to be in accordance with appropriate security regulations.

2*b*. GROUP: Automatic downgrading is specified in DoD Directive 5200.10 and Armed Forces Industrial Manual. Enter the group number. Also, when applicable, show that optional markings have been used for Group 3 and Group 4 as authorized.

3. REPORT TITLE: Enter the complete report title in all capital letters. Titles in all cases should be unclassified. If a meaningful title cannot be selected without classification, show title classification in all capitals in parenthesis immediately following the title.

4. DESCRIPTIVE NOTES: If appropriate, enter the type of report, e.g., interim, progress, summary, annual, or final. Give the inclusive dates when a specific reporting period is covered.

5. AUTHOR(S): Enter the name(s) of author(s) as shown on or in the report. Enter last name, first name, middle initial. If military, show rank and branch of service. The name of the principal author is an absolute minimum requirement.

6. REPORT DATE: Enter the date of the report as day, month, year; or month, year. If more than one date appears on the report, use date of publication.

7*a*. TOTAL NUMBER OF PAGES: The total page count should follow normal pagination procedures, i.e., enter the number of pages containing information.

7*b*. NUMBER OF REFERENCES: Enter the total number of references cited in the report.

8*a*. CONTRACT OR GRANT NUMBER: If appropriate, enter the applicable number of the contract or grant under which the report was written.

8*b*, 8*c*, & 8*d*. PROJECT NUMBER: Enter the appropriate military department identification, such as project number, subproject number, system numbers, task number, etc.

9*a*. ORIGINATOR'S REPORT NUMBER(S): Enter the official report number by which the document will be identified and controlled by the originating activity. This number must be unique to this report.

9*b* OTHER REPORT NUMBER(S): If the report has been assigned any other report numbers *(either by the originator or by the sponsor)*, also enter this number(s).

10. AVAILABILITY/LIMITATION NOTICES: Enter any limitations on further dissemination of the report, other than those imposed by security classification, using standard statements such as:

(1) "Qualified requesters may obtain copies of this report from DDC."

(2) "Foreign announcement and dissemination of this report by DDC is not authorized."

(3) "U. S. Government agencies may obtain copies of this report directly from DDC. Other qualified DDC users shall request through _____."

(4) "U. S. military agencies may obtain copies of this report directly from DDC. Other qualified users shall request through _____."

(5) "All distribution of this report is controlled. Qualified DDC users shall request through _____."

If the report has been furnished to the Office of Technical Services, Department of Commerce, for sale to the public, indicate this fact and enter the price, if known.

11. SUPPLEMENTARY NOTES: Use for additional explanatory notes.

12. SPONSORING MILITARY ACTIVITY: Enter the name of the departmental project office or laboratory sponsoring *(paying for)* the research and development. Include address.

13. ABSTRACT: Enter an abstract giving a brief and factual summary of the document indicative of the report, even though it may also appear elsewhere in the body of the technical report. If additional space is required, a continuation sheet shall be attached.

It is highly desirable that the abstract of classified reports be unclassified. Each paragraph of the abstract shall end with an indication of the military security classification of the information in the paragraph, represented as *(TS)*, *(S)*, *(C)*, or *(U)*.

There is no limitation on the length of the abstract. However, the suggested length is from 150 to 225 words.

14 KEY WORDS: Key words are technically meaningful terms or short phrases that characterize a report and may be used as index entries for cataloging the report. Key words must be selected so that no security classification is required. Identifiers, such as equipment model designation, trade name, military project code name, geographic location, may be used as key words but will be followed by an indication of technical context. The assignment of links, roles, and weights is optional.